Telerehabilitation of a Exoskeleton-haptic device System

Design and Evaluation on Stability and Transparency

N. Korzilius

Msc. Thesis

Motor Learning and Neurorehabilitation lab

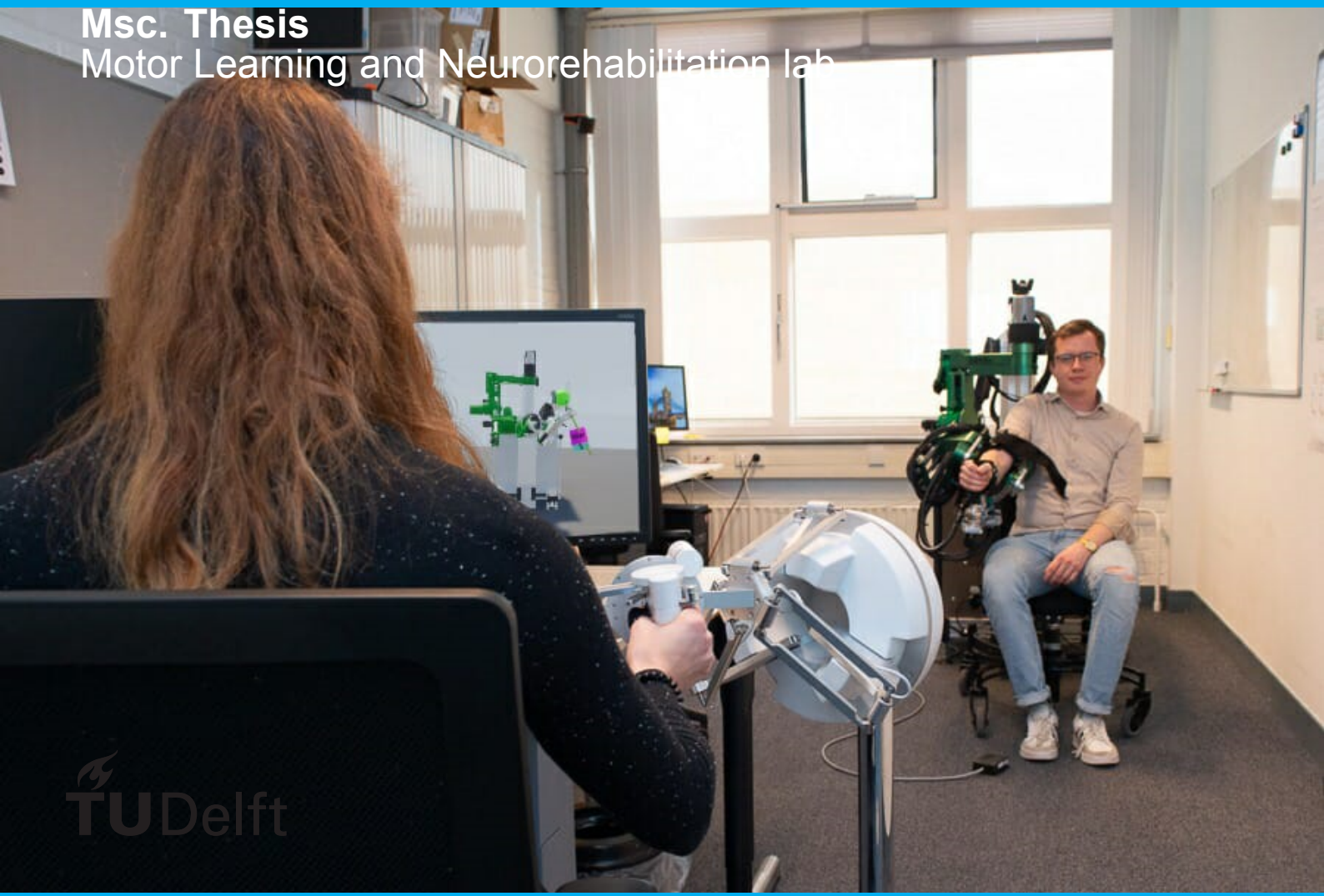

TU Delft

Telerehabilitation of a Exoskeleton-haptic device System

Design and Evaluation on Stability and Transparency

by

N. Korzilius

to obtain the degree of Master of Science
at the Delft University of Technology,
to be defended publicly on Tuesday September 19, 2023 at 9:00 AM.

Student number:	4351762	
Project duration:	December 1, 2022 – September 19, 2023	
Thesis committee:	Dr. ing. L. Marchal Crespo,	TU Delft, chair,supervisor
	Ing. A. van den Berg,	TU Delft, daily supervisor
	Dr. J. Kober,	TU Delft

TU Delft

Preface

The healthcare system is strained, and with an aging population, this problem is more likely to worsen. This is also the case in the field of neurorehabilitation, where the problem is twofold: rehabilitation by therapists and aftercare of non-autonomous patients by nurses both cost manpower. As a technological solution to this problem, robotic rehabilitation devices have been developed. They facilitate high-intensity, autonomous training in a motivating environment. Freeing up the therapist to focus on important non-repetitive tasks of rehabilitation. Additionally, robots can provide more and higher intensity training, giving back more autonomy to the patient and less burden for the nurses.

However, in clinical practice rehabilitation robots are not yet common, and are often underused. In my literature research, I tried to uncover what the shortcomings of these devices are according to therapists. And investigated if haptic communication could solve some of these issues. In this MSc. thesis I designed a tele-rehabilitation system that facilitates haptic interaction between the patient in an upper-extremity exoskeleton and therapist using an end-effector haptic device. And as a proof of concept, evaluate the system on stability and transparency.

This thesis is submitted as part of the requirements of my Master's degree in Robotics at the Delft University of Technology. The research presented was conducted under the supervision of Dr.ing. Laura Marchal-Crespo and Ing. Alex van den Berg at the Department of Cognitive Robotics at the Faculty of Mechanical, Maritime and Materials Engineering. All project code can be found on the Delft University of Technology Gitlab:
https://gitlab.tudelft.nl/mln-lab/unity/mscprojectnkorziliustelerehab/-/tree/V1/FD_Local_control
https://gitlab.tudelft.nl/mln-lab/unity/armin-visualization/-/tree/TeleRehab-VR?ref_type=heads
https://gitlab.tudelft.nl/mln-lab/simulink/arminplus/-/tree/nk_delta?ref_type=heads
All data and code for processing data can be found at the Project Storage of Delft University of Technology:
file://tudelft.net/staff-umbrella/MscProjectNKorziliusTelerehab/

N. Korzilius
Delft, September 2023

Acknowledgements

First I would like to thank my supervisors Laura Marchal-Crespo and Alex van den Berg. I would like to thank Laura for her enthusiasm and feedback on this project, and for giving me the opportunity to come up with my own project. But also for being an amazing role model in a male-dominated industry, you have inspired me and have given me the confidence to make something great from my future career. I would like to thank Alex for all the help during the project, feedback, and discussions, and also for helping me find the internship. I have enjoyed our conversations a lot, whether they were about technology or something completely different. I could not have imagined a better place to graduate, and I am eternally grateful for this opportunity!

I also want to thank Alex Ratschat (MLN lab, TU Delft) for his help with the ARMin V, and Raphael Rätz (ARTORG, Bern University) for all the help with the Force Dimension haptic devices. I also want to thank Luka Peternel (Haptics lab, TU Delft) for his time to discuss teleoperation theory.

Lastly, I would of course like to thank my friends and family for their support throughout my studies.

Contents

1

Scientific Paper

Telerehabilitation Design and Evaluation on Stability and Transparency

Nikki Korzilius, *MSc Student, Delft University of Technology,*

***Abstract*—While the presence and demand of robotic rehabilitation devices are rising, not many studies have been performed on haptic communication/ telerehabilitation with these devices. Despite therapists' desire to have the possibility to remain in the loop when their patients are performing exercises. This study aims to provide a telerehabilitation system that accommodates therapist-patient interaction during robotic rehabilitation and evaluate the system empirically on stability and transparency. The system provides a platform for further research on telerehabilitation and haptic communication in robotic rehabilitation. Working towards a system that allows the therapist, when desired, to intuitively interact with the patient while they are performing rehabilitation exercises using a robotic device. A modular telerehabilitation system is designed using the ARMin V (ETH Zurich) upper extremity exoskeleton as the patient side, and the haptic end-effector device Sigma.7 (Force Dimensions) as the therapist's side. A visualization is provided to the therapist side using Unity and additional features are added to improve usability. The telerehabilitation system is bilateral impedance controlled through a proportional-derivative controller. An experiment is performed in which the observing participant is asked to resist motion (analyze stability) or to be compliant with the motion (analyze transparency). The empirical analysis showed promising first results on position tracking, effective communication of haptic cues, stability, and transparency. However, UDP communication rate could be raised, and the scaling of force and workspace between Sigma.7 and ARMin V could be better matched to improve transparency.**

***Index Terms*—Bilateral, Telerehabilitation, Impedance control, proof of concept, Upper-Extremity.**

I. Introduction

With an aging population, the need for technological improvement in the field of rehabilitation is also rising [1]–[5]. Robots for rehabilitation have been emerging and have been promising with regard to effectiveness in relearning motor skills [6], [7]. They also allow for repetitive training which can be performed mostly independently, allowing the therapist to take a more supervisory role and help several patients at the same time [8]. However, the therapist can only adjust high-level exercise parameters and give verbal feedback to the patient and cannot physically interact with the patient when using the rehabilitation robot due to moving mechanical components [9], [10]. Nonetheless, physical contact is common practice in rehabilitation and also facilitates social contact [11]. To allow interaction between the therapist and the patient when using robots, haptic communication, which can transfer information on dynamics, and kinematics but also intention [12], could be added. This can be done by introducing a haptic display for the therapist. The system could be used for pose correction during exercises (when the amount of connection points has been extended), or to use their expertise to personalize the exercise by either helping or countering movements of the patient [13], [14]. Haptic communication can also provide social facilitation, such as increased performance speed and extended motivation [15].

Manuscript received September 5, 2023; revised August 22, 2023.

Few studies have been conducted on telerehabilitation, and most relied on audio-visual interaction [16]. Klamroth-marganska et al. also concluded that the effectiveness of telerehabilitation still has to be proven, especially using larger groups of participants that also fit the demographic of the end users.

To be able to conduct this research first a telerehabilitation system has to be provided.

We propose a design for a modular telerehabilitation system that allows the therapist to interact with the patient in an upper-extremity exoskeleton. To evaluate the quality of the proposed system design, experiments are performed to evaluate the stability and transparency empirically.

This research consists of a research and design phase and an experiment for a proof of concept. Where we empirically evaluate the system and identify areas of improvement.

First, we will discuss the system design, including functionalities implemented and devices used. Then the experiment for system evaluation is discussed, results of the experiment are shown and discussed. Lastly, shortcomings of the current system and future research projects are discussed.

This study aims to provide a framework for modular telerehabilitation upon which more research, such as motor learning and usability studies, can be performed, eventually providing a platform for therapists to interact with patients while using robotic rehabilitation devices.

II. Methods

System Design

A. System Overview

To provide haptic interaction to the patient using the upper-extremity exoskeleton ARMin V (ETH Zurich) during robotic rehabilitation exercises the therapist is provided with the Sigma.7 (by ForceDimensions) haptic end-effector device which is bilaterally connected to the end-effector of the exoskeleton (Figure 1). An end-effector haptic device was chosen over a second upper-extremity exoskeleton due to its

modular application [1], [8]. The modular approach could provide the therapist with a single system that provides an interface that can be connected to a multitude of different rehabilitation robots with different kinematics. This reduces the number of robots needed in a clinic, but also the number of systems a therapist should be familiar with. The Sigma.7 has seven Degrees of Freedom (DoF): 3 translational, 3 rotational, and 1 in the Gripper (as found on the spec sheet [17]).
The ARMin V moves the shoulder and elbow with 4 DoF's and the forearm with 2 DoF's.
To measure forces exerted by the patient on the ARMin V's force sensors (Schunk Mini45) were attached to the three cuffs.

The therapist is also provided with a visualization of both robots in Unity (Figure 2), as adding visual feedback to haptic communication improves the ability to interpret haptic cues [18], [19]. This visualization was displayed using a Head Mounted Display (HMD) (HTC Vive Pro).

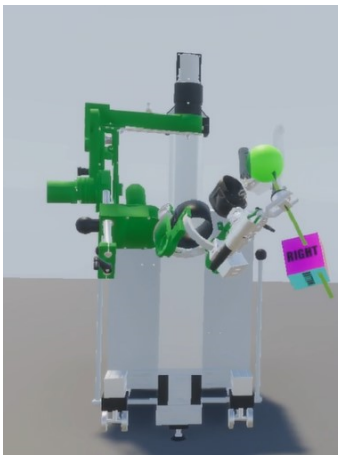

Fig. 2. Visualization of ARMin V and Sigma.7 (cube) with connection point (green sphere) and force vector (line)

Fig. 1. Overview Tele-Rehabilitation System

B. Visualization

For visualization of both robots, Unity (Unity 2021.3.2f1) is used, with the following additional packages: OpenXR Plugin, High Definition RP, and in-lab packages for UDP communication in JSON format. The ARMin V is visualized with a digital twin, a virtual representation of the ARMin V which is updated from real-time data [20]. And Sigma.7 is visualized as a cube with the orientation indicated on its surfaces (Figure 2). As the workspace of the Sigma.7 is significantly smaller than the ARMin V's it is scaled such that the Sigma.7 is able to reach the maximum range of motion of the ARMin V, which was approximated to be a factor 10.

The therapist is provided with visualization through an HMD (Section II-D4).

C. Network

The complete network (Figure 3) consists of three computers connected to each other through a network switch (tp-link 8-port Gigabit, TL-SG108) using Ethernet cables.

The ARMin V is executed from an 'XPC-Target' computer (Spectra GmbH & Co. KG, RAM: 2 GB, CPU: Intel Core 2, 3 GHz) running a Simulink model launched from a 'Host' computer (OS: Windows 10, RAM: 32 GB, NVIDIA GeForce RTX 2080 Ti). On the Host computer, we also run the visualization in Unity. Due to limitations in the amount of UDP connections of Simulink, we use Unity to chain the UDP connection to the tertiary computer, also named the Linux computer, (OS: Ubuntu 18.04, RAM: 512 GB, NVIDIA GV102) from where the teleoperation control is run, and the Sigma.7 is connected.

The following information is sent between the computers:
Target to Host:

- Position and orientation (ARMin V).

Host to Target:

- Force and torque from teleoperation controller (ARMin V)

Linux to Host:

- Position and orientation (Sigma.7)
- Force and torque from teleoperation controller (ARMin V)
- Graspflag

Host to Linux:

- Position and orientation (ARMin V)
- Camera-angle

1) UDP Communication:

The communication is done through the User Datagram Protocol (UDP).

Simulink has an update rate of 3kHz for both the control of ARMin V and the UDP communication with the Host computer. The UDP communication in Unity is done in separate threads to detach their speed from Unity's update rate. However, this was not implemented correctly for the connection with the Linux computer, causing the Host computer to send UDP packages at only 88 Hz.

Update rates were calculated by recording UDP connections on Wireshark (Wireshark.org, https://www.wireshark.org/) (filtered for connections). All the connections are recorded on the host computer, additionally, Linux-Host UDP connections are also recorded on the Linux computer.

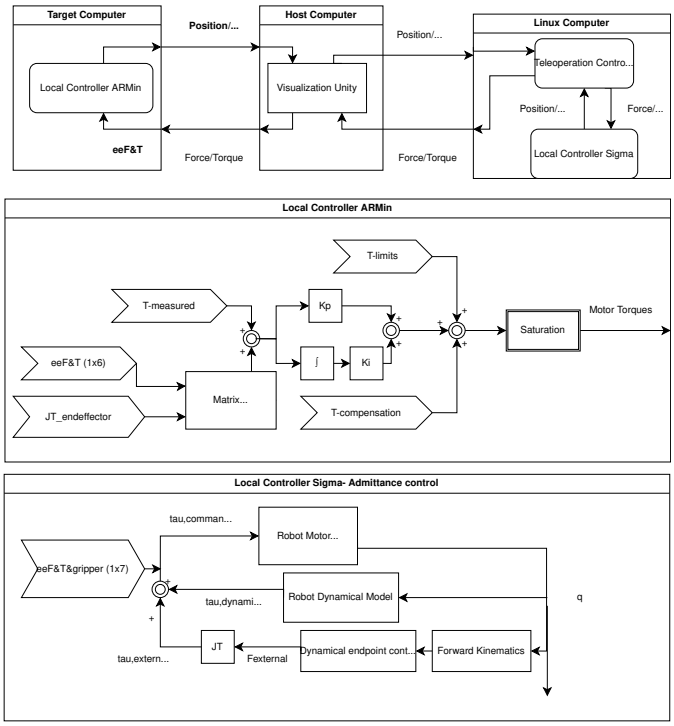

Fig. 3. Schematic of teleoperation network and local controllers

D. System Features

Software should be easy and intuitive to use for both therapist and patient [21]. Thus some basic features were added with usability in mind.

1) Grasp to connect:
To let the patient perform the exercises without haptic interaction, and only provide haptic interaction when desired, the system is built so that the therapist can grasp the connection point (see Figure 2) to start the teleoperation control. The teleoperation controller uses the position/orientation of the connection point and returns force/torque to be exerted on the connection point. Grasping is implemented by having the end-effectors in proximity (10 cm in ARMin V workspace, 1 cm in Sigma.7 workspace) to each other in the visualization combined with the closing of the gripper of the Sigma.7. To indicate the activity of the connection a binary variable 'Graspflag' is sent to Unity causing the connection point to change color to green when grasped. Once grasped the proximity of the end-effectors is not checked anymore, otherwise, the teleoperation control would stop when the distance between the end-effectors is larger than 10 cm in ARMin V's workspace. To let go of the ARMin V the therapist has to open the gripper. 3 N is constantly applied to the index finger on the gripper of the Sigma.7, keeping the gripper open unless consciously closed. For this study, only one connection point has been implemented at the end-effector of ARMin V. This method can be extended to multiple grasping points in order to be able to correct poses and assess different muscles.

2) Force Vector:
To provide the therapist with more context of the force applied to the patient a force vector has been visualized. This is done by visualizing a line starting from the ARMin V end-effector in the direction of the force and with scaled length relative to the magnitude of the force. The force vector is also provided with a discrete color gradient (green, orange, red) to represent a magnitude between 0-30 N, concurrently informing the therapist of the magnitude of the force.

3) Camera Rotation:
Not all exercises performed by the patient will be clear from the frontal plane, and thus another point of view might be desired. To provide the therapist with a better view of the interaction, the therapist can rotate the camera around the Z-axis of the origin of the coordinate of the ARMin V (Figure 4) using left and right keyboard arrows. The local coordinate frame of Sigma.7 follows this rotation in Unity, making sure that the movement of Sigma.7 remains the same relative to the display. Consequently, the rotation needs to be accounted for when transposing the end-effector position of Sigma.7 from its local coordinate frame to the local coordinate frame of the ARMin V before end-effector positions can be input into the teleoperation controller (Section II-E1).

This rotation can only be done when the therapist is not grasping the patient. This will prevent sudden unwanted forces applied to both devices when rotating.

4) Head Mounted Display:
It was chosen to display the visualization to the therapist on an HMD, as the use of an HMD could improve the spatial insight of the interaction compared to using a computer monitor [22], and thus improve the usability of the system. The point of view displayed on the HMD follows the movement of the head and has to be re-centered upon startup of the system using the space bar on the keyboard.

E. Teleoperation Controller

1) Coordinate Frames:
All calculations are made with respect to ARMin V's coordinate frame (a). Therefore the end-effector position of the Sigma.7 ($\vec{X}_s$) is transformed to ARMin V's frame. As described in Section II-D4, the coordinate frame of the Sigma.7 can rotate with the virtual camera of the visualization around the ARMin V with an angle β (β >0 when rotating anti-clockwise) around the Z-axis. This results in the rotation matrix:

$$R_{S,A} = \begin{bmatrix} cos(-\beta) & sin(-\beta) & 0 \\ -sin(-\beta) & cos(-\beta) & 0 \\ 0 & 0 & 1 \end{bmatrix} \quad (1)$$

Furthermore, to match workspaces of both robots the Sigma.7's workspace is scaled with C_{scale}=10. To match the coordinate system origins of both robots before rotation, an offset upon initialization is taken into account. This offset was introduced to best match the differently shaped workspaces of the robots, the following values were used as the offset [0.34 m,0 m,1 m]. This results in a total transformation of Sigma.7's local coordinate frame to ARMin V's local coordinate frame in Equation 2.

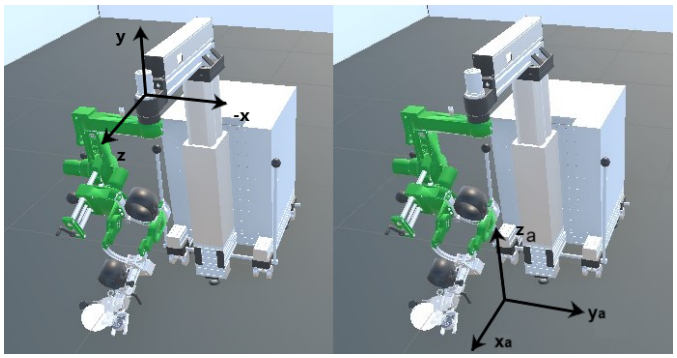

Fig. 4. Coordinateframes ARMin V, Left Unity, Right ARMin V's controller frame

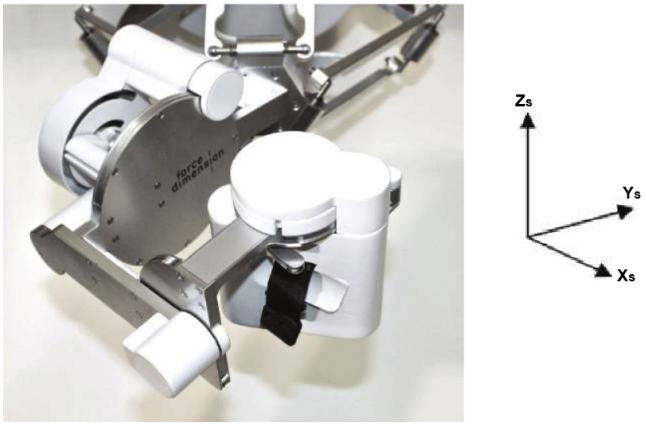

Fig. 5. Coordinateframe Sigma.7, as found in user manual

$$\vec{X'}_{a,s} = C_{scale} \cdot \vec{X}_s \cdot R_{S,A} + \begin{bmatrix} x_{offset} \\ y_{offset} \\ z_{offset} \end{bmatrix} * R_{S,A} \qquad (2)$$

2) Controller:

To pick the right type of controller we need to keep the application in mind. The focus of robotic rehabilitation devices is relearning motor functions, and learning can be described as a collaborative process [18] between teacher and student.

The patient requires the interaction forces provided by the therapist for her/his learning [19], while the therapist requires the interaction forces between the patient and the robot to estimate participation, but also stiffness from the arm [23]–[25] to prevent going beyond the patient's range of motion.

Thus a bilateral teleoperation control scheme was chosen, meaning that both the therapist and patient influence and feel interaction forces and torques. As the therapist requires force to estimate stiffness and a difference in size and shape of the workspaces for both robots is present, impedance control was chosen over admittance control. Impedance control is implemented using a proportional-derivative (PD) algorithm, which functions as a spring-damper system between the two end-effectors. However, due to the kinematic structure of the ARMin V (six DoF) there are no redundant degrees of freedom when controlling force and torque simultaneously, which could result in reaching singularities. A safety layer in the local ARMin V controller needs to be added to deal with these singularities before force and torque can be controlled simultaneously. Thus two separate controllers were designed, one for torque-orientation control (Equation 4 and 6) and one for force-position (Equation 3 and 5) control. Both controllers were designed and tested separately, but this paper will only include results from force-position control. For results on torque-orientation control, the reader is referred to Appendix B. The following equations were used as the teleoperation control equations, with $_P$: patient (ARMin V) and $_t$: therapist (Sigma.7).

TABLE I
PD VALUES, $_P$: PATIENT (ARMIN V) AND $_t$: THERAPIST (SIGMA.7), $_F$ FOR FORCE-POSITION CONTROL AND $_\tau$ FOR TORQUE-ORIENTATION CONTROL

$P_{F,p}$	30.0	N/m
$P_{F,t}$	15.0	N/m
$D_{F,p}$	0.01	Ns/m
$D_{F,t}$	0.015	Ns/m
$P_{\tau,p}$	0.002	Nm/deg
$P_{\tau,t}$	0.0044	Nm/deg
$D_{\tau,p}$	0.00	Nms/deg
$D_{\tau,t}$	0.00001467	Nms/deg

$$\vec{F}_p = -P_{F,p} * (\vec{x}_p - \vec{x}_t) - D_{F,p} * (\dot{\vec{x}}_p - \dot{\vec{x}}_t) \qquad (3)$$

$$\vec{\tau}_p = -P_{\tau,p} * (\vec{\theta}_p - \vec{\theta}_t) - D_{\tau,p} * (\dot{\vec{\theta}}_p - \dot{\vec{\theta}}_t) \qquad (4)$$

$$\vec{F}_t = -P_{F,t} * (\vec{x}_t - \vec{x}_p) - D_{F,t} * (\dot{\vec{x}}_t - \dot{\vec{x}}_p) \qquad (5)$$

$$\vec{\tau}_t = -P_{\tau,t} * (\vec{\theta}_t - \vec{\theta}_p) - D_{\tau,t} * (\dot{\vec{\theta}}_t - \dot{\vec{\theta}}_p) \qquad (6)$$

All vectors are 3 Dimensional:

- End-effector position vector: $\vec{x} = [x\ y\ z]^T$
- Orientation vector: $\vec{\theta} = [\theta_x\ \theta_y\ \theta_z]^T$
- Force vector: $\vec{F} = [F_x\ F_y\ F_z]^T$
- Torque vector: $\vec{\tau} = [\tau_x\ \tau_y\ \tau_z]^T$

The PD values chosen can be found in Table I. Separate P and D values are chosen for force and torque controllers as their state-force relation is different. The gain for P was chosen through empirical testing, such that is high enough to properly feel the feedback and the robots move upon the force application, but not too high such that it would be safe.
The gain for D was calculated based upon Lee and Spong's [26] Equation 7 for energetic passive bilateral teleoperation with a constant time delay, assuming the time delay is relatively constant. Energetic passivity is defined as consuming energy, but not producing energy. Where τ_{rt} (6.67*E-4 s) is the round trip time delay between the two robots, which can be estimated using the worst delay found by performing a ping test on the network, or by the worst Δt between messages of the UDP communication.

$$K_D = \frac{\tau_{rt}}{2} * K_P \qquad (7)$$

EXPERIMENT

To evaluate the telerehabilitation system, a small proof of concept study was performed. Teleoperation systems are often evaluated on their stability and transparency (e.g., [27]–[29]). Stability is important for the safety of human operators and robots. Transparency is important to be able to accurately perceive the resistance to motion (impedance) of the patient [14]. Stability and transparency analysis is often performed theoretically, using impedance models and local controller parameters [27], [30]. However, since the impedance models of the robots and local control parameters for the Sigma.7 are unknown the system is analyzed empirically.

As the patient and therapist are also part of the telerehabilitation system, two healthy young human participants (one male, one female) performed the experiment. The participants gave their informed consent prior to the experiment, and the telerehabilitation system and experiment were approved by the ethics committee of the Delft University of Technology. Both participants were part of the Motor Learning and Neurorehabilitation lab and were familiar with haptic devices and HMDs.

F. Tasks

In teleoperation, hard and soft contact operations are used to evaluate transparency and stability [31]. The environment with which a teleoperation system is in contact is inanimate and approached using a spring constant. However, the environment of the telerehabilitation system is the human arm inside the exoskeleton, which cannot be approached by a spring constant. This is similar to the haptic end-effector device, where the environment of the haptic end-effector (in this case the Sigma.7) is the therapist. Hard contact could be translated to the participant resisting motion provided by the other participant, approaching as high as possible stiffness of the human arm, and achieving minimal movement. Soft contact for teleoperation is free movement or compliant contact. This translated to active and passive following of the motion by the human operator for rehabilitation. Since human operators are an inherent part of the system, their impedance models cannot be omitted from the analysis.

The participants are either asked to be a demonstrator (demonstrating the motion) or an observer (responding to the provided motion). To evaluate the system from both Sigma.7 to ARMin V and ARMin V to Sigma.7, the roles are switched. The system is evaluated by performing two types of exercises: compliant and resistive (Table II).

TABLE II
EXPERIMENT TASK OVERVIEW

	Demonstrator	Observer
Resistive	Sigma.7	ARMin V
	ARMin V	Sigma.7
Compliant Passive	Sigma.7	ARMin V
	ARMin V	Sigma.7
Compliant Active	Sigma.7	ARMin V
	ARMin V	Sigma.7

1) Resistive Task:
In the resistive task, the observer resists movement in the x, y, and z directions provided by the demonstrator. Then observer and demonstrator roles are switched and the task is repeated.

2) Compliant Tasks:
With the compliant task, the observer follows the motion provided by the demonstrator, and both participants take on the demonstrator and observer roles. The demonstrator is asked to provide a motion that makes use of all three DoF's and aims at multiple movements that use multiple DoF's at the same time (such as diagonal or spiraling movement) but do not follow a predefined path.

The compliant evaluation consists of both the passive and active behavior of the participant who observes the demonstration.

In *passive compliant behavior* the participant is asked to do nothing, there is no resistance or movement provided by the participant. The participant is not activating their muscles during the task. We chose to evaluate passive compliant behavior because telerehabilitation contains two humans, and the impedance of the human arm should be taken into account when evaluating the entire system. When evaluating compliant passive operation we eliminate the influence of the human operator's input to position or force and purely evaluate the position and force tracking based on actuation of the robots.

While in *active compliant behavior* the participant is asked to follow the movement provided by the demonstrator. It is important to note that the participant in the ARMin V has no visualization available and thus follows movement purely based on experienced forces produced by the teleoperation controller. The participant controlling the Sigma.7 is thus asked to close their eyes after connecting the devices to avoid following the movement based on visualization rather than based on forces perceived. We chose to evaluate active compliant behavior as this is closest to the purpose of the system in clinical practice. Additionally, when comparing active and passive compliant behavior we can gain insight into if the force cues are interpretable by the observer.

G. Stability

Stability is empirically analyzed based on the force tracking errors, defined as $F_{controlled} - F_{Measured}$, from the resistive task. A frequency analysis of the tracking errors is also performed, in which we evaluate their magnitude and frequency. Furthermore, the lag between the two end-effector signals is calculated by taking the lag (in the number of samples) at the maximum cross-correlation and multiplying this by the mean time difference between samples.

H. Transparency

1) Position Tracking:
To evaluate the transparency based on position tracking the position-tracking error between the two end-effectors is calculated, and normalized over the range of motion of the observer. The scaled end-effector position and workspace for the Sigma.7 are used for these calculations. Delay in position tracking is calculated the same as mentioned in stability.

2) Impedance Ratio:
According to [27], [30] transparency is the accurate transmission of impedance. In a classic teleoperation system, this is approached by $\frac{Z_{transmitted}}{Z_{environment}}$, with $Z_{transmitted} = \frac{F_h}{V_h}$, where F represents force and V represents velocity and $_h$ represents the human operator, and $Z_{environment} = \frac{F_e}{V_e}$, where $_e$ represents the environment which is another human operator for the telerehabilitation system. Lawrence and Hashtrudi & Zaad [27], [30] approach the impedance ratio mathematically in the frequency domain by using the robots' impedances and local and teleoperation control gains. However, the impedances of Sigma.7 and ARMin V are unknown, and we thus approach the impedance ratio empirically. Transparency is thus evaluated by position tracking errors between the end-effectors and the impedance ratio (Equation 8). In this case, the transmitted impedance is approached by the demonstrator's impedance and the environment impedance by observer impedance, using measured position and force from both robots. Velocity (v) is calculated using the measured position and time difference.

$$\frac{Z_{demonstrator}}{Z_{observer}} = \frac{(F_{demonstrator}/v_{demonstrator})}{(F_{observer}/v_{observer})} \tag{8}$$

To evaluate the impedance ratio in the frequency domain first, we take the force and velocity Fourier transform and then apply Equation 8. Ideal transparency is achieved if the magnitude of the impedance ratio is 1, and the phase is 0.

I. Data Collection

1) Recorded Data:
Force, torque, position, and orientation are all measured on both robots. Measured force and torque for the ARMin V are obtained from the force sensor on the end-effector, while the Sigma.7 estimates force and torque from motor current. The position and orientation for the ARMin V are found using the potentiometers and forward kinematics, the Sigma.7 presumably also uses forward kinematics to find the position and orientation of the end-effector. The measured force and torque of ARMin V are in the opposite direction of the controlled force as the sensor measures the interaction force/torque of the human on the end-effector. Data is captured on both sides of the system. On the computer running Sigma.7 the following variables are recorded:

- Measured Force Sigma.7 (x,y,z)
- Time
- Measured Torque Sigma.7 (x,y,z)

On the host computer of the ARMin V, the following variables are recorded:

- Force-measured ARMin V(x,y,z)
- Joint torques (Joint 1-6)
- Teleoperation torques (Joint 1-6)

Where teleoperation torques are the end-effector forces from the teleoperation control (x,y,z) transposed to the joint space of the ARMin V with the Jacobian of the end-effector. Joint torques are the summation of the three force sensor measurements transposed to the joint space. All information that is communicated over the UDP connections is also recorded (Section II-C1).

2) UDP Communication:
To analyze the stability of the network itself the UDP communication is also captured using Wireshark. These captures are saved as .csv files and can be analyzed in Matlab. Here the average, minimum, and maximum time between messages, as well as the average communication frequency are calculated.

3) Videos:
To create a better insight into all features and performance of the total system videos were recorded during the experiment. These were: screen capture of Unity, frontal view of ARMin V, and back view of the Sigma.7.

III. Results

Because the experiments were performed with both participants using the Sigma.7 and ARMin V taking on both demonstrator and observation roles, there will be two datasets per task (resistive, compliant passive, and compliant active). To differentiate between the two sets per task we used the demonstrator (either Sigma.7 or ARMin V) to mark the results.

A. Communication Update-rate

The UDP update rate is assessed to evaluate the quality of the network connection itself. The results are averaged per task and then averaged over all tasks. In Table III can be seen that all connections achieve a high update frequency except for the Host to Linux connection.

TABLE III
UDP Updaterates (dt [s]), * marks location of recording

Sender	Receiver	Max (dt)	Min (dt)	avg (dt)	avg (freq)
Linux	Host*	2.5E-02	0	3.1E-04	3211
Linux*	Host	4.3	1.28E-05	4E-04	2950
Target	Host*	6.2E-02	1.33E-06	2.2E-04	4803
Host*	Target	2.2E-02	3.33E-07	3E-04	3372
Host*	Linux	1.7	9E-03	1.1E-02	89
Host	Linux*	3.5	9E-03	1.1E-02	88

B. Stability

To analyze stability we assess the resistive task (which is selected as the telerehabilitation equivalent of hard contact analysis, see Section II-F and II-G) on oscillatory behavior. Both participants took on the observer and demonstrator roles.

1) Force Tracking Error, Time Domain:
We are mostly interested in how the measured forces behave, as the measured forces are a result of the combination of the entire system including the local controller and human arm.

From Figures 6 and 7 we can see the reaction forces based on the displacement of the demonstrator. Notable are the forces in the X-direction in Figure 6 while there is no displacement of the Sigma.7, and the relatively small magnitude of the force of the Sigma.7 in Figure 7. This resulted in the force tracking errors in Table IV, which shows large errors between demonstrator and observer and between controlled and measured forces for the ARMin V. Additionally, the delay between the demonstrator and the observer based on the measured forces through cross-correlation is given in Table V.

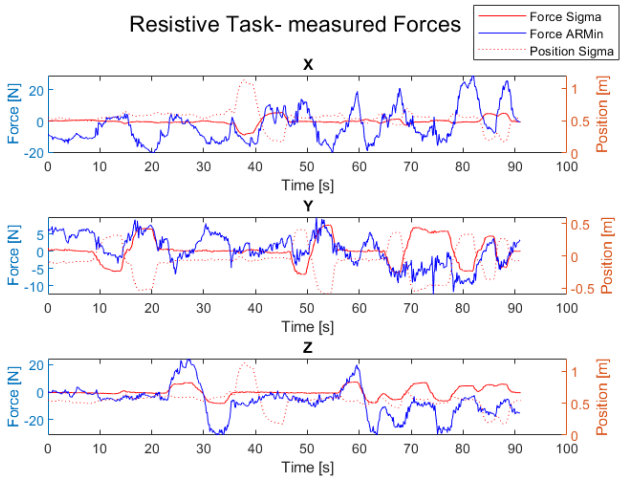

Fig. 6. Measured Forces Resistive, Demonstrator Sigma.7

Fig. 7. Measured Forces Resistive, Demonstrator ARMin V

TABLE IV
FORCE TRACKING ERRORS IN TIME DOMAIN

Demonstrator: Sigma		**X**	**Y**	**Z**
$F_{demonstrator,measured}$- $F_{observer,measured}$	mean [N]	9.7	4.9	11
	std [N]	11.4	6.4	13.9
Fcontrol-Fmeasured (ARMin)	mean [N]	16.8	15.7	16.7
	std [N]	19.6	20.9	17.1
Fcontrol-Fmeasured (Sigma)	mean [N]	2E-4	1.9E-4	1.4E-4
	std [N]	3.8E-4	2.8E-4	3.1E-4
Demonstrator: ARMin		**X**	**Y**	**Z**
$F_{demonstrator,measured}$- $F_{observer,measured}$	mean [N]	13.8	14	15.2
	std [N]	17.1	18.4	15.7
Fcontrol-Fmeasured (ARMin)	mean [N]	14.1	11.2	12
	std [N]	13.3	14.2	13
Fcontrol-Fmeasured (Sigma)	mean [N]	2E-4	1.9E-4	1.4E-4
	std [N]	3.8E-4	2.8E-4	3.1E-4

TABLE V
FORCE TRACKING LAG [S] BETWEEN OBSERVER & DEMONSTRATOR (MEASURED)

	X	Y	Z
Dem: Sigma	0.3633	0.1845	-0.2299
Dem: ARMin	3.4149	0.1394	3.1686

2) Frequency Analysis:
To analyze the stability during the resistive task we look at the force tracking error in the frequency domain. The force tracking error analyzed here is $F_{ARMin-controlled} - F_{ARMin-Measured}$ as the force tracking error of Sigma.7 is negligible (see Table IV). As the velocity of Sigma.7 was filtered with a cut-off frequency of 15 Hz the force tracking error in the frequency domain is only analyzed up to this cut-off frequency.

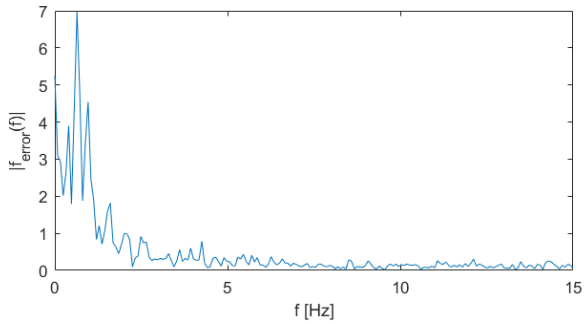

Fig. 8. Frequency analysis force tracking error, Demonstrator: Sigma.7

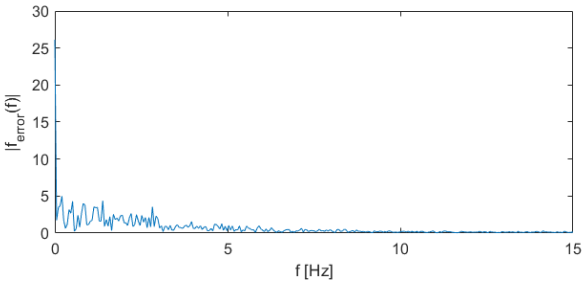

Fig. 9. Frequency analysis force tracking error, Demonstrator: ARMin V

C. Transparency

To analyze the transparency of the system we analyze a compliant passive and compliant active task on position tracking as well as the impedance ratio. To analyze if position tracking errors present are caused by a workspace mismatch the workspace of the observer is marked on Figures 10,11,12 and 13 by red lines for all axis. The timing of position tracking is analyzed using the delay found based on cross-correlation in Table VII. Negative values were found when the Sigma.7 was demonstrating, this could be explained by the mismatch in workspaces when scaled. The Sigma.7 is able to reach positions in ARMin V's workspace that the ARMin V cannot reach, causing the movement of the observer to stop before

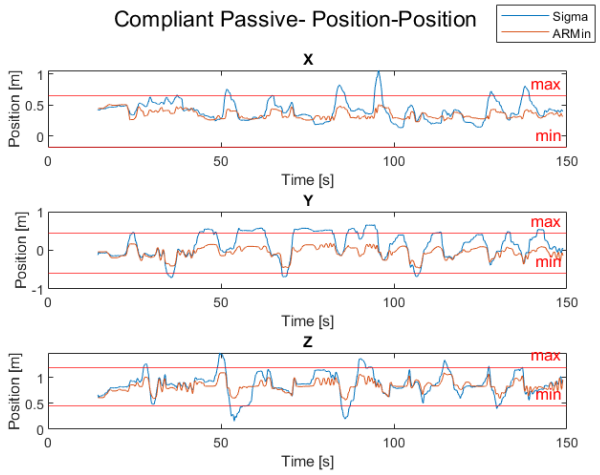

Fig. 10. Position tracking, Demonstrator: Sigma.7

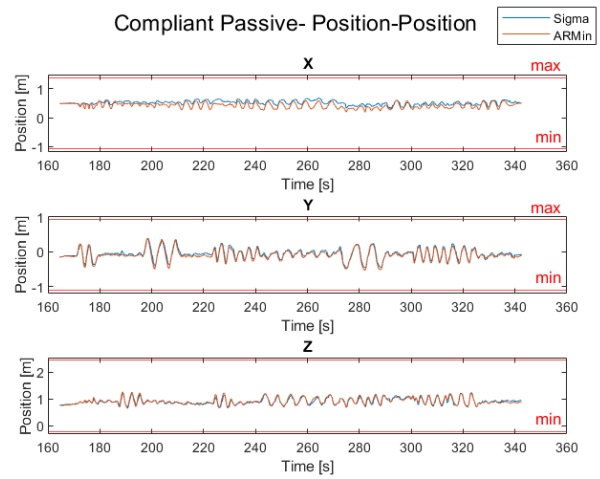

Fig. 11. Position tracking, Demonstrator: ARMin V

the demonstrator's. When employing the cross-correlation algorithm it could find the maximum cross-correlation on such a point and return a negative lag indicating the observer is ahead of the demonstrator.

1) Tracking Errors:

Absolute tracking error is calculated in percentage of the observer's ROM, which is scaled in the case of Sigma.7, and given by mean and standard deviation in Table VI.

2) Impedance Ratio:

Due to the use of a lowpass filter for the velocity of Sigma.7 to remove aliasing, it was chosen to only investigate the impedance ratio up to the chosen cut-off frequency of 15 Hz.

Fig. 12. Position tracking, Demonstrator: Sigma.7

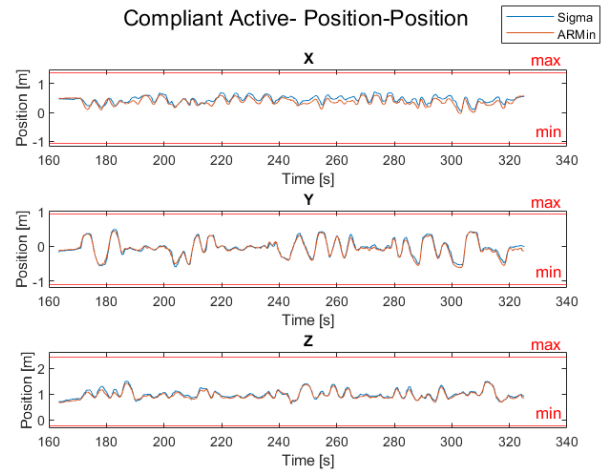

Fig. 13. Position tracking, Demonstrator: ARMin V

TABLE VI
POSITION TRACKING ERRORS AS PERCENTAGE OF ROM OBSERVER [%]

		X	Y	Z
Compliant Passive Dem: Sigma.7	**mean**	12.259	21.195	15.1113
	std	11.0734	16.1154	13.349
Compliant Passive Dem: ARMin V	**mean**	3.8551	1.956	1.1605
	std	2.2777	1.3377	0.9171
Compliant Active Dem: Sigma.7	**mean**	11.9734	12.2521	13.6672
	std	12.5942	8.7599	11.1932
Compliant Active Dem: ARMin V	**mean**	3.3983	1.7427	1.6061
	std	1.8701	1.3578	1.0437

TABLE VIII
IMPEDANCE RATIO MAGNITUDE [-]

Data set	mean	std	median
Compliant Passive Dem: Sigma.7	1.468	2.3618	0.1806
Compliant Passive Dem: ARMin V	2.3893	3.5266	0.952
Compliant Active Dem: Sigma.7	12.8924	29.8924	0.3839
Compliant Active Dem: ARMin V	1.3695	1.2545	1.1525

TABLE VII
POSITION TRACKING LAG [S] BASED ON CROSS-CORRELATION

Dataset	dt X	dt Y	dt Z
Compliant Passive Dem: Sigma	-0.2548	-0.2548	-0.2548
Compliant Passive Dem: ARMin	0.2556	0.2606	0.175
Compliant Active Dem: Sigma	-0.1354	-0.1354	-0.1354
Compliant Active: Dem: ARMin	0.2635	0.2439	0.1594

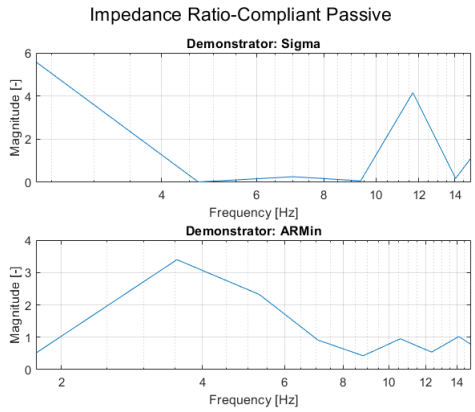

Fig. 14. Impedance Ratio, Compliant Passive

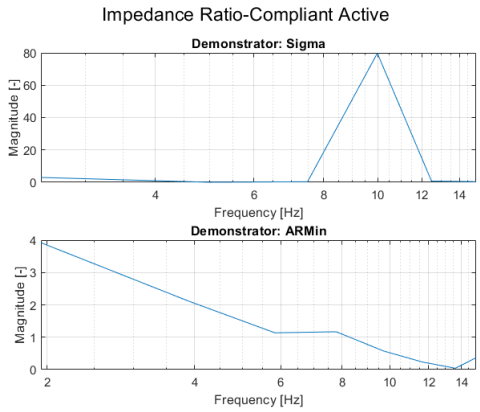

Fig. 15. Impedance Ratio, Compliant Active

IV. DISCUSSION

A. UDP update-rate

When evaluating the UDP update rates (Table III) most noticeable is the update rate from Host to Linux around 88 Hz. This can be attributed to Unity's MonoBehaviour update rate, to which the UDP communication with Linux was attached, which was set to 100 Hz as increasing this rate did not result in improved UDP communication. This would also mean that even though Linux sends messages to the Host computer with a frequency of around 3 kHz, Unity updates its visualization and forwards the message to the UDP sender for the target computer with the same internal update rate. So even though the ARMin V's local control is at 3 kHz and Sigma.7's local control is up to 4 kHz, teleoperation control runs at 88H z, which is lower than the desired order of E^3. A lower frequency constitutes a higher sensorimotor delay, which if significant leads to instability and an untransparent system [30]. According to Madder et al. [32] delay up to 250 ms is imperceptible by the human, and with the lowest frequency being 88 Hz the system is still well below the perceivable delay. Sensorimotor delay can be further influenced by the time delay caused by physical distance, which would be introduced into the system when used as a telerehabilitation system, causing the system to move away from stability. To ensure stability under constant time-delay a passivity controller based on energetic passivity could be implemented [26].

It is thus desired to improve the UDP connection between the Host and Linux computer, either by improving the connection in Unity or by detaching the communication between both robots from the visualization.

B. Stability

When looking at the results of the resistive task we found that the measured force of the Sigma.7 is relatively low, and deviates very little from the controlled force of the Sigma.7. The control forces for both the Sigma.7 and ARMin V are well-damped and do not show any oscillations that are not caused by displacement.

1) Force Tracking Error, Time Domain:

Demonstrator: Sigma.7, Observer: ARMin V
Inspecting Figure 6 we see that the measured force of the ARMin V follows a similar shape as the measured force of the Sigma.7. However, in Table IV we see a large force tracking error, especially in the X (9.7 N) and Z (11.0 N)-directions. Force tracking lag (Table V) is relatively low with values between 0.18-0.36 s. A negative lag value would mean the observer is ahead of the demonstrator at the point of highest cross-correlation, which is most likely an issue with using the cross-correlation for finding lag. In the X-axis we can see a force response even though no movement in this axis is provided. This is due to the joint kinematics of ARMin V that require movement in other axes in addition to the desired movement.

Demonstrator: ARMin V, Observer: Sigma.7
Looking at Figure 7 we can see that the measured force of the ARMin V tracks the shape of its position well. However, measured force for the ARMin V reaches values of magnitude 40 N while the measured force of the Sigma.7 stays below 10 N. This difference in measured force can also be seen in Table IV for both mean and standard deviation in all directions compared to when Sigma.7 is demonstrating. This large difference between the measured forces of the observer and demonstrator could also explain the large values for lag in the X (3.4 s) and Z (3.2 s) directions, as maximum cross-correlation is more likely to occur when the magnitude of the force of ARMin V is 0 N then when it is reacting to displacement. Reducing the force tracking error between the Sigma.7 and ARMin V could be achieved by increasing the proportional gain K_p for the Sigma.7, which is currently half the proportional gain for the ARMin V (Table I).

2) Force Tracking Error, Frequency Domain::
Control forces of both the ARMin V and Sigma.7 do not display oscillations, while ARMin V's measured forces show oscillations. Additionally, the force tracking error of Sigma.7 (E-4, Table IV) was negligible. Thus it was chosen to analyze the force tracking error of ARMin V in the frequency domain.

Demonstrator: Sigma.7, Observer: ARMin V
From the frequency analysis (Figure 8), it can be seen that the highest magnitude of force tracking error for the ARMin V is 7 N at 0.64 Hz. The magnitude of the force tracking error quickly drops with higher frequencies and is already below 1N at 2.57 Hz.

Demonstrator: ARMin V, Observer: Sigma.7
From the frequency analysis (Figure 9), we can see the highest magnitude at 0 Hz of 26.1 N, meaning a constant bias is present. This can be seen most clearly in Figure 7 in the X and Z-axes, where an oscillation offset is clearly visible as the force in the positive direction reaches 40 N while in the negative direction -20 N.

Furthermore, the magnitude of the force error is still at 3.5 N around 2.8 Hz, which could correlate with the instability seen during a compliant passive task when Sigma.7 was demonstrating. An instability was noticed between the 60-80 s mark in Figure 10. Best seen in the Y and Z-axis where the position of Sigma.7 remains fairly constant but the position of ARMin V oscillates.

The low-frequency instability could be explained by the impedance of the human arm which is more compliant to displacement in low-frequency than high-frequency force applied. The frequency of the instability could also be low enough to not disturb the absolute stability of the system. From Dong et al. [33] we found that the hand-arm system resonates most in the frequency range of 20 to 50 Hz. From van der Helm et al. [34] it was concluded that frequencies < 3 Hz would not excite the eigenfrequency of the closed-loop system (hydraulic manipulator and human arm).

C. Transparency

1) Tracking Errors:
Due to the nature of both devices, they both have different workspaces and maximum force/torque. Therefore, a scaling of the workspace from Sigma.7 to the ARMin V has been applied (factor 10). However, there is still a mismatch in the shape of the workspace between ARMin V and Sigma.7. Additionally, Sigma.7 is limited to a maximum force of 20 N, this is too small a force to move the ARMin V.
But when looking at force tracking between the ARMin V and the Sigma.7 (Figure 7) we can see that the gain K_p of Sigma.7's teleoperation control should be higher, as ARMin V is able to reach a maximum force of 54 N, while Sigma.7 was only able to reach 11 N.

a) Compliant Passive Tasks:
Demonstrator: Sigma.7, Observer: ARMin V
When looking at Figure 10, we can see that the ARMin V follows the movement of the Sigma.7 with a lag of 0.25 s (Table VII). However, ARMin V is unable to follow the end-effector position of the Sigma.7 to its full extent. This can be explained by the workspace of ARMin V for the X and Z directions (see Figure 4 for reference), which are restricted in the negative X and Z direction by the participant's body, and restricted in the positive X and Z direction by the total arm length (0.65 m) of the ARMin V. Lastly in the Y direction, even though the workspace did not limit the position tracking, during the experiments it was noticed that the shoulder joint of the ARMin V (which is the most dominant joint for movement in the Y direction) was only slightly moving when high forces were exerted. This could be explained by the inertia of the shoulder joint being too high to move with the desired speed by the controlled forces applied. Resulting in a relatively high mean position tracking error and large standard deviation (Table VI).

Demonstrator: ARMin V, Observer: Sigma.7
When looking at Figure 11, we can see that the Sigma.7 is tracking the position of the ARMin V very well. However, in the X-axis it can be seen that even though the timing of the Sigma.7 following the ARMin V is accurate (0.26 s, Table VII), the actual magnitude of displacement (position tracking error of 3.8 %, Table VI) does not match.

When comparing the mean and standard deviation of the Position tracking error for Sigma.7 to ARMin V and ARMin V to Sigma.7 in Table VI, we see that when Sigma.7 is observing it is able to track the demonstrator better than when ARMin V is observing.

b) Compliant Active Task:
When looking at the compliant active position tracking we are mostly interested in how well the observer is able to interpret and act upon the haptic cues. As this would be closer to the application in rehabilitation.

Demonstrator: Sigma.7, Observer: ARMin V
When comparing Figures 12 and 13 it seems that position tracking is improved, especially in the Y axis. This is confirmed by Table VI, here position tracking error for the passive task was 21.2 % and only 12.2 % for the active task. These results seem to relate to the issues with high inertia of the shoulder joint mentioned in the compliant passive task. But for the active task forces felt by the participant in the ARMin V seem to give enough information to track the position as demonstrated. Additionally, position tracking lag is almost halved compared to the passive case (Table VII).

Demonstrator: ARMin V, Observer: Sigma.7
Similar to the compliant passive task the Sigma.7 is able to follow the position of ARMin V very well (Figure 13). When comparing the position tracking error for the passive and active task (Table VI) barely any improvement in position tracking can be seen. Additionally, the position tracking lag barely improved compared to the passive case (Table VII).

2) Impedance Ratio:
With impedance ratio, we are analyzing how well the observer is able to perceive the impedance of the demonstrator (Equation 8). Ideal transparency is achieved with an impedance ratio of magnitude 1. When looking at Figures 14 & 15 we see the impedance ratio is not constant over frequency and is far from the ideal magnitude of 1. Additionally from Table VIII we can see a large standard deviation for all tasks, indicating an inconsistent transmission of impedance. This can

be explained by a combination of lag in the system (Table V VII) and the complexity of the human arm. The human arm has seven DoF, and multiple muscles in multiple orientations that influence the impedance depending on the orientation of the arm and muscle activation. Thus when there is a delay in the system causing different orientations of the demonstrator's and observer's arms, a difference in impedance is to be expected. Reducing the tracking error in force and position and thus in impedance ratio could give a more consistent impedance ratio. This could be achieved by tuning the control parameters, or by adding an integral gain K_i to the teleoperation controller.

a) Compliant Passive Tasks:

Demonstrator: Sigma.7, Observer: ARMin V

For the compliant passive task when the Sigma.7 is demonstrating we see a mean magnitude of impedance ratio of 1.468 (Table VIII), and a standard deviation of 2.4. From Figure 14 it can be seen that the impedance ratio for analyzed frequencies is either close to 0 or between 4-6. An impedance of close to zero could be caused by a high observer impedance. While an impedance around 5 can be explained by the choices made in the scaling of workspace and force. We expect an impedance ratio of 5 due to this scaling without taking into account the robot's local controllers and the different kinematic properties.

Demonstrator: ARMin V, Observer: Sigma.7

Looking at Figure 14 we see that for most frequencies the impedance ratio is close to 1, however with 2 larger outliers the mean (2.4) and standard deviation (3.5) are larger than expected. Furthermore, with higher frequencies, the impedance ratio is closer to 1. Indicating that the system becomes more transparent for higher frequencies.

b) Compliant Active Tasks:

Demonstrator: Sigma.7, Observer: ARMin V

When comparing the magnitude of the impedance ratio with the compliant passive task we see a similar behavior of impedance ratio. However, the outlier at 10 Hz in Figure 15 is much higher. This causes a high mean and standard deviation in Table VIII The impedance ratio for all other analyzed frequencies is close to 1, and improved compared to the compliant passive case. **Demonstrator: ARMin V, Observer: Sigma.7**

Comparing the compliant active task to the compliant passive task (Table VIII)when ARMin V is demonstrator we see that the active task is performing better on transparency. Additionally comparing Figures 14 to 15 the impedance ratio takes on a very different behavior over frequencies. However, for both tasks the impedance ratio improves with higher frequencies.

D. General Remarks

When comparing the measured forces of the observers to the position and force of the demonstrator it is visible that in addition to force/movement in the desired axis forces/movement in other axes are also present. This is most noticeable in the ARMin V, which due to the six joint-link structure requires movement in another axis to achieve the movement of the desired axis. Furthermore, forces measured for the ARMin V are only measured in the end-effector to compare how well the force is applied to the end-effector. However, to move the ARMin V to the desired position force is not only applied to the end-effector but also to other joints. From the results, it was noticeable that the position scaling for Sigma.7 could be lower. The Sigma.7 was able to go outside of ARMin V's workspace, which is undesired. Additionally could reduce the impedance ratio of the system when Sigma.7 is demonstrating, which is currently four times higher than the ideal impedance ratio of magnitude one.

Comparing the compliant passive results (Figure 10)with the compliant active results (Figure 12) we see improved tracking for the ARMin V as an observer when the participant is actively participating. This is especially visible on the Y-axis. The shoulder joint of the ARMin V is responsible for most of the movement on the Y-axis but also requires the highest joint torque to move. This is due to the inertia of the total ARMin V that needs to be overcome to move the shoulder joint. When inspecting Figure 10 it is evident that the teleoperation control forces are not high enough to overcome this inertia and move the joint with the desired speed. This could be improved by using a more transparent local controller for the ARMin V. Or by implementing the kinematic model of the ARMin V in the teleoperation controller as a feed-forward element to ensure that returned joint torques are high enough.

E. Shortcoming of the System

Due to the use of local controllers and their safety layers for both robots, the effect of teleoperation control gain K_D is unclear. This is due to the fact that the local controllers already stabilize with dampening before forces and torques are applied. To see the effects of K_D we can only look at the forces coming out of the teleoperation control algorithm, which showed no oscillatory behavior.

Furthermore, torque-orientation control is not evaluated in this paper. Though the orientation of certain points in the arm can play an essential role in rehabilitation, it cannot be combined with force-position control due to a current lack of singularity safety layers in the ARMin V, as the amount of DoF's of the ARMin V(six) is the same as the desired controlled amount of DoF's. While the end-effector orientation of the haptic device is independent of its position, this is not the case for the ARMin V, which depends on its joint positions and orientation to reach a particular end-effector orientation. The end-effector torque calculated is then translated over to the different joints. However, some joints have higher inertia and thus require higher torque to move than others.

F. Future Works

Due to the scope of the project, many observations and ideas are still left for the future, such as a user experience experiment, which could also contain other points of view in the visualization. But could also research if haptic communication contributes to social facilitation in robotic rehabilitation. And a motor learning experiment to review the influence of haptic communication on motor learning when using robotic rehabilitation. To use the system for actual telerehabilitation (therapist not in the same room/building/city as the patient) stability under large time delay needs to be researched. This

could also be achieved by adding a stabilizing method to the controller.

Furthermore, some improvements in the design came to light. More points to 'grab' the exoskeleton with the haptic device would also be desirable for more possibilities of therapist-patient interaction. Another option that could be investigated is how Sigma.7 connects to a point on the exoskeleton. e.g. by following a connection point and connecting with a keyboard press, and changing connection points with another keyboard press.

Control gains of the current controller could be optimized. Different teleoperation controllers could also be implemented and compared to achieve higher transparency and stability. A safety layer could be implemented on the ARMin V local controller that prevents reaching singularity configurations so that it can be driven both in torque and force simultaneously.

V. Conclusion

The experiments showed promising first results with regard to position tracking, clarity of haptic cues in the compliant active task, stability in higher frequencies, and transparency. The results also indicated some limitations of the current system.

For low frequencies, the force tracking error displayed a large magnitude. However, no high-frequency components seem to be prominent. The system showed stable behavior, except for low-frequency instability as seen in Figure 10 around the 60-80 s mark.

When the Sigma.7 was observing a lower position tracking errors were present, and the impedance was perceived more accurately than when the ARMin V was observing. The impedance ratio was inconsistent and could be improved by reducing the delay, or by reducing force and position tracking errors by tuning the control parameters. Even with these limitations, very promising tracking is visible in the compliant active task (Figures 12 and 13). Showing the potential of the haptic cues provides enough context to communicate kinematics to the observer.

Even though the telerehabilitation system did not display any instabilities (other than the low-frequency instability mentioned above), the UDP update rate should be improved. A higher update frequency should contribute to a more stable system, which is important when introducing time delay.

With an increasing need for rehabilitation and a decreasing number of therapists, we can expect an increase in robots for rehabilitation to fill this gap. But by using robots for rehabilitation we remove the interaction with the therapist. This study tries to provide a modular system to allow for interaction with the therapist while still leaving the premises of robotic rehabilitation intact. In this study, a first design for a modular telerehabilitation system is set up and tested on stability and transparency. Due to the scope of the study, many studies could be performed on the system. Such as fine-tuning control parameters, adding torque control, stability analysis under large time delay with stabilizing methods, a user experience experiment, and research if haptic communication contributes to social facilitation and motor-learning experiments. But there is also much room for extension of the current system, such as more connection points for the systems, different points of view for the therapist, and different controllers.

References

[1] H. I. Krebs and N. Hogan, "Therapeutic robotics: A technology push," *Proceedings of the IEEE*, vol. 94, no. 9, pp. 1727–1737, 2006, ISSN: 00189219. DOI: 10.1109/JPROC.2006.880721.

[2] G. Kwakkel, B. J. Kollen, and H. I. Krebs, "Effects of robot-assisted therapy on upper limb recovery after stroke: A systematic review," *Neurorehabilitation and Neural Repair*, vol. 22, no. 2, pp. 111–121, 2008, ISSN: 15459683. DOI: 10.1177/1545968307305457.

[3] C. R. Carignan and H. I. Krebs, "Telerehabilitation robotics: Bright lights, big future?" *Journal of Rehabilitation Research and Development*, vol. 43, no. 5, pp. 695–710, 2006, ISSN: 07487711. DOI: 10.1682/JRRD.2005.05.0085.

[4] T. Tao, X. Yang, J. Xu, *et al.*, "Trajectory Planning of Upper Limb Rehabilitation Robot Based on Human Pose Estimation," *2020 17th International Conference on Ubiquitous Robots, UR 2020*, pp. 333–338, 2020. DOI: 10.1109/UR49135.2020.9144771.

[5] N. Takeuchi and S. I. Izumi, *Rehabilitation with post-stroke motor recovery: A review with a focus on neural plasticity*, 2013. DOI: 10.1155/2013/128641.

[6] S. Masiero, P. Poli, G. Rosati, *et al.*, "The value of robotic systems in stroke rehabilitation," *Expert Review of Medical Devices*, vol. 11, no. 2, pp. 187–198, 2014, ISSN: 17434440. DOI: 10.1586/17434440.2014.882766.

[7] S. Dehem, M. Gilliaux, G. Stoquart, *et al.*, "Effectiveness of upper-limb robotic-assisted therapy in the early rehabilitation phase after stroke: A single-blind, randomised, controlled trial," *Annals of Physical and Rehabilitation Medicine*, vol. 62, no. 5, pp. 313–320, 2019, ISSN: 18770665. DOI: 10.1016/j.rehab.2019.04.002.

[8] A. Akbari, F. Haghverd, and S. Behbahani, "Robotic Home-Based Rehabilitation Systems Design: From a Literature Review to a Conceptual Framework for Community-Based Remote Therapy During COVID-19 Pandemic," *Frontiers in Robotics and AI*, vol. 8, no. June, pp. 1–34, 2021, ISSN: 22969144. DOI: 10.3389/frobt.2021.612331.

[9] J. Lanini, T. Tsuji, P. Wolf, R. Riener, and D. Novak, "Teleoperation of two six-degree-of-freedom arm rehabilitation exoskeletons," *IEEE International Conference on Rehabilitation Robotics*, vol. 2015-Septe, pp. 514–519, 2015, ISSN: 19457901. DOI: 10.1109/ICORR.2015.7281251.

[10] K. Baur, N. Rohrbach, J. Hermsdorfer, R. Riener, and V. K. Marganska, "The "Beam-Me-In" Strategy Remote Haptic Therapist- Patient Interaction with Two Exoskeletons for Stroke Therapy," *International Journal of Physical Medicine & Rehabilitation*, vol. 06, no. 02, pp. 1–15, 2018. DOI: 10.4172/2329-9096.1000464.

[11] V. Klamroth-marganska, J. G. Schönhammer, S. Giovanoli, and C. A. Easthope, "Telerehabilitation : Technology transforms Neurorehabilitation after Stroke," pp. 1–38,

[12] R. Groten, D. Feth, R. L. Klatzky, and A. Peer, "The role of haptic feedback for the integration of intentions in shared task execution," *IEEE Transactions on Haptics*, vol. 6, no. 1, pp. 94–105, 2013, ISSN: 19391412. DOI: 10.1109/ToH.2012.2.

[13] M. H. Koh, S. C. Yen, L. Y. Leung, *et al.*, "Exploiting telerobotics for sensorimotor rehabilitation: a locomotor embodiment," *Journal of NeuroEngineering and Rehabilitation*, vol. 18, no. 1, pp. 1–21, 2021, ISSN: 17430003. DOI: 10.1186/s12984-021-00856-w. [Online]. Available: https://doi.org/10.1186/s12984-021-00856-w.

[14] S. Lennon, "Physiotherapy practice in stroke rehabilitation: A survey," *Disability and Rehabilitation*, vol. 25, no. 9, pp. 455–461, 2003, ISSN: 09638288. DOI: 10.1080/0963828031000069744.

[15] K. B. Reed and M. A. Peshkin, "Physical collaboration of human-human and human-robot teams," *IEEE Transactions on Haptics*, vol. 1, no. 2, pp. 108–120, 2008, ISSN: 19391412. DOI: 10.1109/TOH.2008.13.

[16] V. Klamroth-marganska, S. Giovanoli, and C. A. Easthope, *Telerehabilitation Technology*. Springer International Publishing, 2022, ISBN: 9783031089954. DOI: 10.1007/978-3-031-08995-4. [Online]. Available: http://dx.doi.org/10.1007/978-3-031-08995-4_25.

[17] F. Dimension, *Sigma.7 Haptic Device*, 2019. [Online]. Available: https://www.forcedimension.com/images/doc/specsheet_-_sigma7.pdf.

[18] A. Chellali, C. Dumas, and I. Milleville-Pennel, "Haptic communication to support biopsy procedures learning in virtual environments," *Presence: Teleoperators and Virtual Environments*, vol. 22, no. 1, pp. 470–489, 2013, ISSN: 10547460.

[19] D. Morris, T. Hong, F. Barbagli, T. Chang, and K. Salisbury, "Haptic feedback enhances force skill learning," *Proceedings - Second Joint EuroHaptics Conference and Symposium on Haptic Interfaces for Virtual Environment and Teleoperator Systems, World Haptics 2007*, pp. 21–26, 2007. DOI: 10.1109/WHC.2007.65.

[20] T. Lomba and L. Marchal-Crespo, "Development of an upper limb exoskeleton digital twin in immersive virtual reality," Universidade de Lisboa, Tech. Rep., 2023.

[21] L. Li, S. Tyson, and A. Weightman, "Professionals' Views and Experiences of Using Rehabilitation Robotics With Stroke Survivors: A Mixed Methods Survey," *Frontiers in Medical Technology*, vol. 3, no. November, 2021. DOI: 10.3389/fmedt.2021.780090.

[22] E. D. Ragan, R. Kopper, P. Schuchardt, and D. A. Bowman, "Studying the effects of stereo, head tracking, and field of regard on a small-scale spatial judgment task," *IEEE Transactions on Visualization and Computer Graphics*, vol. 19, no. 5, pp. 886–896, 2013, ISSN: 10772626. DOI: 10.1109/TVCG.2012.163.

[23] J. M. Veerbeek, A. C. Langbroek-Amersfoort, E. E. Van Wegen, C. G. Meskers, and G. Kwakkel, "Effects of Robot-Assisted Therapy for the Upper Limb after Stroke: A Systematic Review and," *Neurorehabilitation and Neural Repair*, vol. 31, no. 2, pp. 107–121, 2017, ISSN: 15526844. DOI: 10.1177/1545968316666957.

[24] R. Bertani, C. Melegari, M. C. De Cola, A. Bramanti, P. Bramanti, and R. S. Calabrò, "Effects of robot-assisted upper limb rehabilitation in stroke patients: a systematic review with meta-analysis," *Neurological Sciences*, vol. 38, no. 9, pp. 1561–1569, 2017, ISSN: 15903478. DOI: 10.1007/s10072-017-2995-5.

[25] T. Richard Nichols and M. Huyghues-Despointes, "Muscular Stiffness," in *Encyclopedia of Neuroscience*, 2009, pp. 2515–2519.

[26] D. Lee and M. W. Spong, "Passive bilateral teleoperation with constant time delays," *Proceedings - IEEE International Conference on Robotics and Automation*, vol. 2006, no. 2, pp. 2902–2907, 2006, ISSN: 10504729. DOI: 10.1109/ROBOT.2006.1642142.

[27] D. A. Lawrence, "Stability and Transparency in Bilateral Teleoperation," *IEEE Transactions on Robotics and Automation*, vol. 9, no. 5, pp. 624–637, 1993, ISSN: 1042296X. DOI: 10.1109/70.258054.

[28] M. Sharifi, S. Behzadipour, and H. Salarieh, "Nonlinear Bilateral Adaptive Impedance Control with Applications in Telesurgery and Telerehabilitation," *Journal of Dynamic Systems, Measurement and Control, Transactions of the ASME*, vol. 138, no. 11, pp. 1–16, 2016, ISSN: 15289028. DOI: 10.1115/1.4033775.

[29] G. Bauer, Y. J. Pan, and H. Shen, "Adaptive Impedance Control in Bilateral Telerehabilitation with Robotic Exoskeletons," *Conference Proceedings - IEEE International Conference on Systems, Man and Cybernetics*, vol. 2020-Octob, pp. 719–725, 2020, ISSN: 1062922X. DOI: 10.1109/SMC42975.2020.9282882.

[30] K. Hashtrudi-Zaad and S. E. Salcudean, "Transparency in time-delayed systems and the effect of local force feedback for transparent teleoperation," *IEEE Transactions on Robotics and Automation*, vol. 18, no. 1, pp. 108–114, 2002, ISSN: 1042296X. DOI: 10.1109/70.988981.

[31] C. N. Mokogwu, K. Razi, and K. Hashtrudi-Zaad, "Experimental Assessment of Absolute Stability in Bilateral Teleoperation," *IEEE Transactions on Haptics*, vol. 13, no. 2, pp. 380–392, 2020, ISSN: 23294051. DOI: 10.1109/TOH.2019.2949819.

[32] R. D. Madder, S. VanOosterhout, A. Mulder, *et al.*, "Network latency and long-distance robotic telestenting: Exploring the potential impact of network delays on telestenting performance," *Catheterization and Cardiovascular Interventions*, vol. 95, no. 5, pp. 914–919, 2020, ISSN: 1522726X. DOI: 10.1002/ccd.28425.

[33] R. G. Dong, T. W. McDowell, and D. E. Welcome, "Biodynamic response at the palm of the human hand subjected to a random vibration," *Industrial Health*, vol. 43, no. 1, pp. 241–255, 2005, ISSN: 00198366. DOI: 10.2486/indhealth.43.241.

[34] F. C. Van Der Helm, A. C. Schouten, E. De Vlugt, and G. G. Brouwn, "Identification of intrinsic and reflexive components of human arm dynamics during postural control," *Journal of Neuroscience Methods*, vol. 119, no. 1, pp. 1–14, 2002, ISSN: 01650270. DOI: 10.1016/S0165-0270(02)00147-4.

A

Teleoperation Structure

A teleoperation structure was built to connect the end effectors of the ARMin V and the Sigma.7 through haptics. This consisted of several parts: UDP communication with and without JSON in Simulink (ARMin V computer), C# (Host computer) and CPP (Sigma.7 computer), a visualization in Unity, Teleoperation in CPP, and lastly translating forces from end effector cartesian forces to motor torque for the ARMin V.

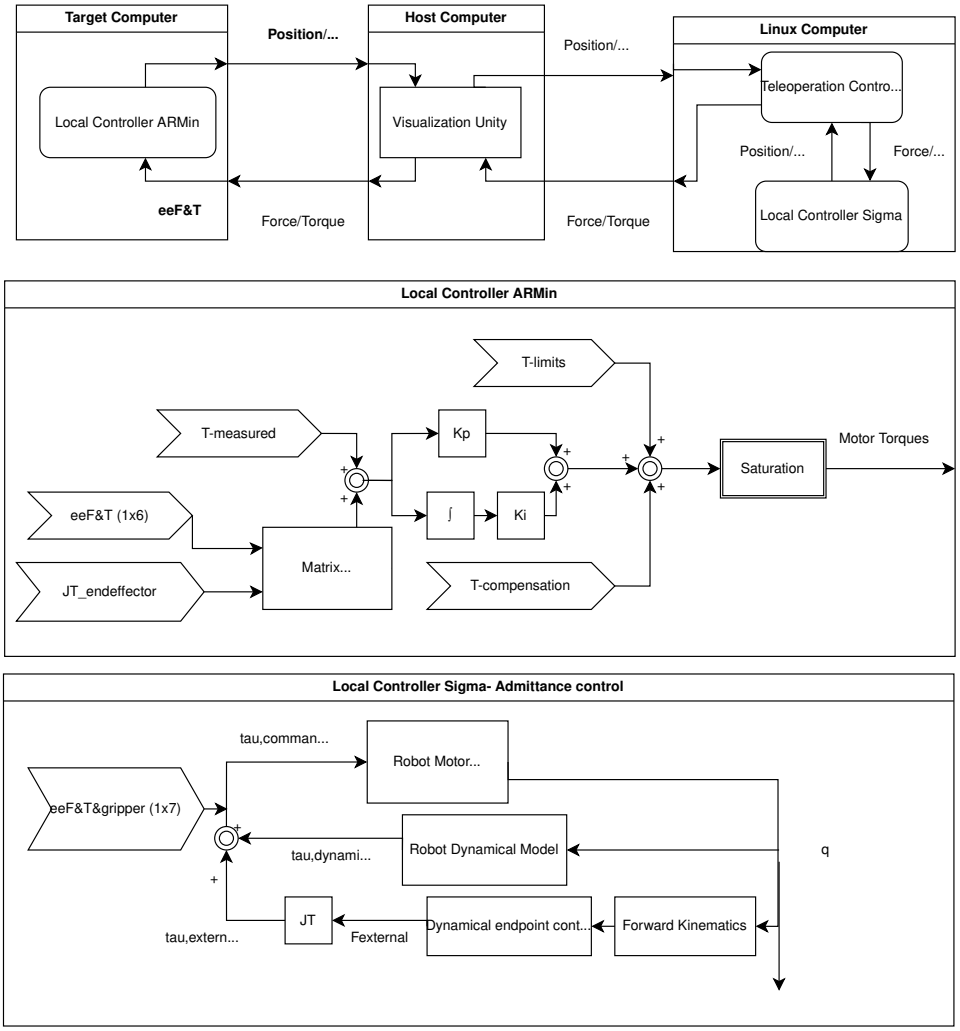

Figure A.1: Schematic of teleoperation network and local controllers

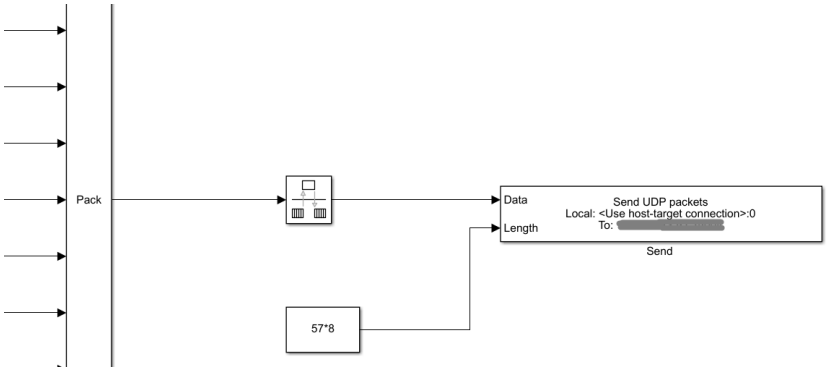

Figure A.2: Simulink UDP (Target-Host connection)

A.1. UDP Communication

For the ARMin V Host -Target communication the already existing Simulink udp communication was used, as can be seen in Figure A.2. In Unity two methods of UDP communication take place: a Target-Host connection (in bytes, separate threading from graphics loop) and a Host-Linux connection (in JSON, linked to graphics loop update rate). In Unity is also where the information between the Sigma.7 and ARMin V is exchanged. Force and torque information for the ARMin V is passed from the Linux receiving connection to the Target sending connection. And position and orientation from the ARMin V end-effector are passed from the Target receiving thread to the Linux sending connection. On the Linux computer UDP communication is done in JSON in CPP, using the UDP CPP library from the MLN lab.

A.2. Unity-Features

The visualization (Figure A.3) was built in Unity (Unity 2021.3.2f1) using the virtual twin of ARMin V by Lomba and Marchal-Crespo, 2023. Added on top of the existing project were added: UDP communication in JSON with the Linux computer, a parser between the two UDP communication with Linux and Host computers, a visualization of the Sigma.7 end effector, a visualization of the exerted force, a visualization of the grasping point, and keyboard-based rotation of the camera.

A.2.1. Sigma.7 End-effector

The end-effector of the Sigma.7 is visualized as a cube with a different color and direction on each face to help the user with orientation (Figure A.4). The cube moved with scaled (factor 10) x,y, and z Cartesian coordinates, and input from Sigma.7 was obtained through UDP communication with the Linux computer.

A.2.2. Force Vector

As there is a scaling between forces (proportional gain K_P for ARMin V is twice as high as for the Sigma.7) and visual cues help interpret haptic cues (Morris et al., 2007), we chose to add a visualization of the force exerted on ARMin V. The force vector displays the direction of the force, and its magnitude through length and color gradient.

A.2.3. Grasping Point

To prevent high forces from arising upon the startup of the program it was chosen to activate teleoperation by the therapist virtually grasping the ARMin V. As only teleoperation to the ARMin V end-effector has been implemented this will be the only grasping point. To indicate where the therapist (user of Sigma.7) is able to hold the ARMin V, a translucent grey sphere is placed at the end effector of the ARMin V. When the Sigma.7 touches the sphere (diameter of 10 cm) and closes the gripper of the Sigma.7 the sphere will turn green and the teleoperation control loop is entered. Due to the scope of this project, only one point has been implemented. However, more of these points are desired to increase the functionality of the system, as more points could enable the therapist to correct the pose of the patient during robotic rehabilitation.

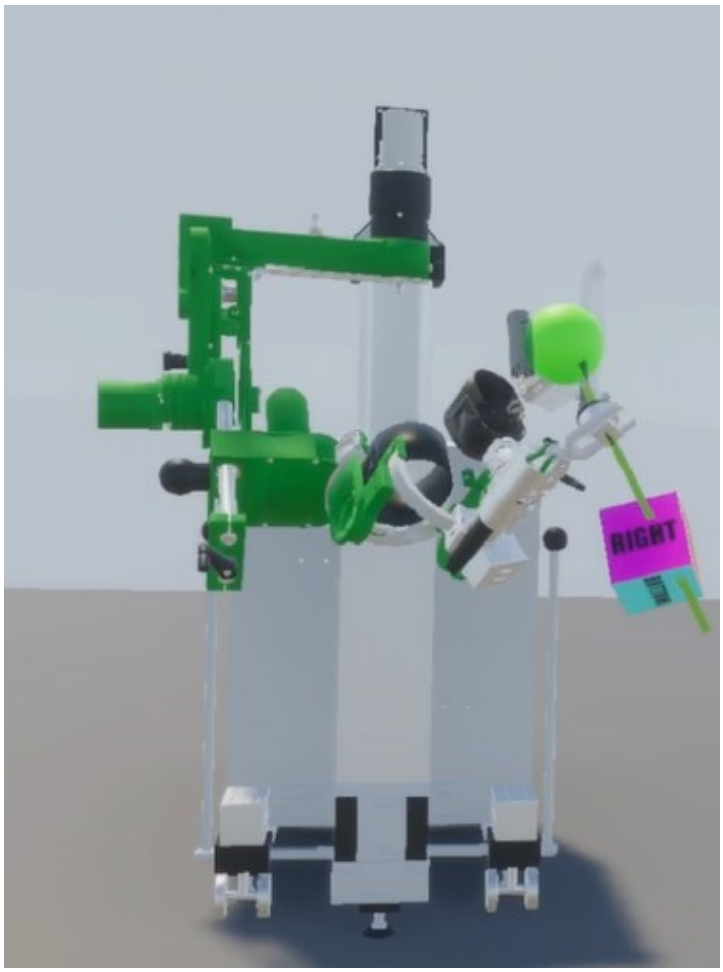

Figure A.3: Visualization Telerehabilitation System in Unity

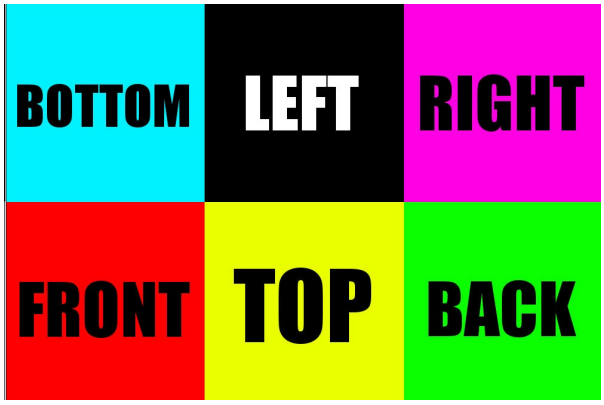

Figure A.4: Cube faces used for end-effector visualization Sigma.7

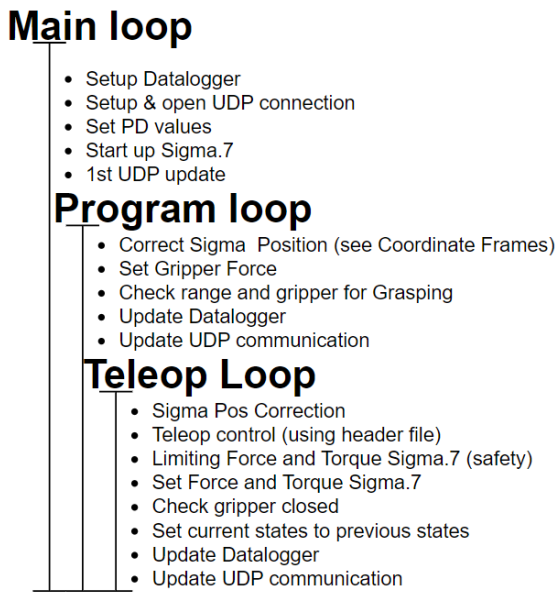

Figure A.5: Structure Control Program

A.2.4. Camera Rotation

To give a better view of different axes a camera rotation was built in. The camera can be rotated around the origin of ARMin V (in Unity) on a radius in the X-Y plane using the keyboard arrow left and right. The end-effector visualization of the Sigma.7 also rotates with the camera, such that the movement of the Sigma.7 relative to the visualization is always the same. As the radius is set only the offset angle of rotation is communicated back to the teleoperation controller on the Linux computer, where the position of the Sigma.7 is corrected before being input into the control algorithm.

A.3. Teleoperation

A.3.1. Coordinate frames

To use the teleoperation control algorithm we first must match the coordinate frames of ARMin V and Sigma.7 so that a position difference can be calculated. The translation of coordinate frames exists of 3 parts: scaling of workspace Sigma.7, offset between origins ARMin V and Sigma.7, and lastly the workspace of Sigma.7 can rotate, with the camera, around the origin of ARMin V. First, the rotation matrix, where β is the camera angle (which is negative when going clockwise) around the Z axis. Scaling is done with C_{scale}=10. The offset is in ARMin Vs' workspace scale and depends on the cube offset used in Unity.

$$R_{S,A} = \begin{bmatrix} cos(-\beta) & sin(-\beta) & 0 \\ -sin(-\beta) & cos(-\beta) & 0 \\ 0 & 0 & 1 \end{bmatrix}$$

$$\vec{X'}_{a,s} = C_{scale} \cdot \vec{X}_s \cdot R_{S,A} + \begin{bmatrix} x_{offset} \\ y_{offset} \\ z_{offset} \end{bmatrix} * R_{S,A} \tag{A.1}$$

A.3.2. Control Loop

The main structure and teleoperation control are done in one CPP file on the Linux computer. This follows the following structure as seen in Figure A.5. The program uses a header file that contains the control algorithm, this makes it easier to alter the control method in the future.

A.3.3. Teleoperation Control

In the header file, we calculate the forces (or torque) from the position (or orientation). This is done using impedance control which is implemented using a PD controller. This leads to the following formula's A.2,A.3, A.4 and A.5. P-D values chosen can be found in table A.1.

Impedance model for the patient (ARMin V):

$$F_p = -P_{F,p} * (x_p - x_t) - D_{F,p} * (\dot{x_p} - \dot{x_t}) \tag{A.2}$$

$$\tau_p = -P_{\tau,p} * (\theta_p - \theta_t) - D_{\tau,p} * (\dot{\theta_p} - \dot{\theta_t}) \tag{A.3}$$

Impedance model for the therapist (Sigma.7):

$$F_t = -P_{F,t} * (x_t - x_p) - D_{F,t} * (\dot{x_t} - \dot{x_p}) \tag{A.4}$$

$$\tau_t = -P_{\tau,t} * (\theta_t - \theta_p) - D_{\tau,t} * (\dot{\theta_t} - \dot{\theta_p}) \tag{A.5}$$

$P_{F,p}$	30.0
$P_{F,t}$	15.0
$D_{F,p}$	0.01
$D_{F,t}$	0.015
$P_{\tau,p}$	0.002
$P_{\tau,t}$	0.0044
$D_{\tau,p}$	0.00
$D_{\tau,t}$	0.00001467

Table A.1: PD values

A.4. Simulink

A.4.1. ARMin V end-effector force

To transpose the end effector force, in cartesian coordinates, to joint torques, in joint space, to actuate the ARMin V it is transformed using the jacobian. This is done using Equation A.6 with $\tau_{J,Teleop}$ is (1x6), JT_{S3} is (6x6), eeF is (1x6) containing also eeτ.

$$\tau_{J,Teleop} = JT_{S3} * eeF \tag{A.6}$$

B

Torque-Orientation Control

As mentioned in the scientific paper it was not possible to control the ARMin V end-effector in both orientation and position at the same time due to safety issues regarding singularities. Thus both components were implemented separately. During the experiment torque-orientation control was tested, however not evaluated in the scientific paper.

B.1. Torque-Orientation Plots, Resistive

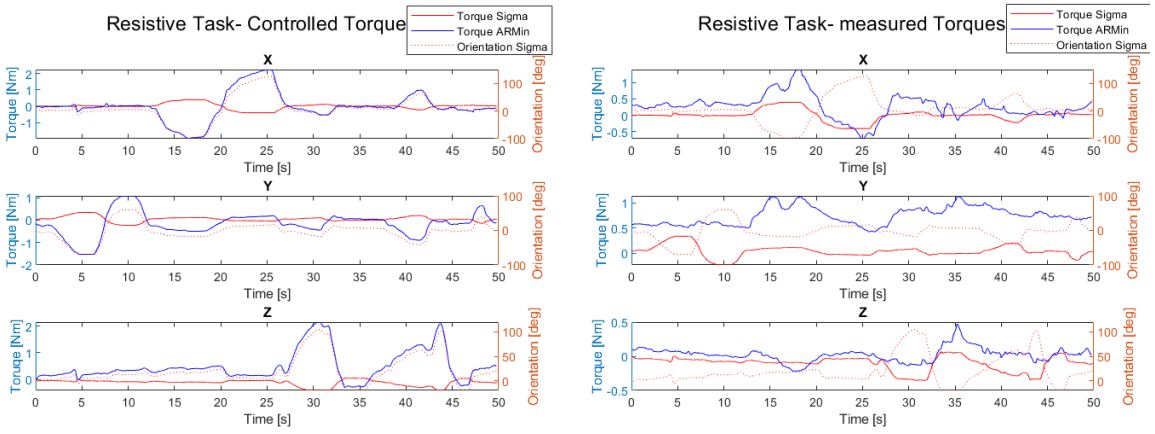

(a) Controlled

(b) Measured

Figure B.1: Torque Orientation plots, Resistive, Demonstrator: Sigma.7

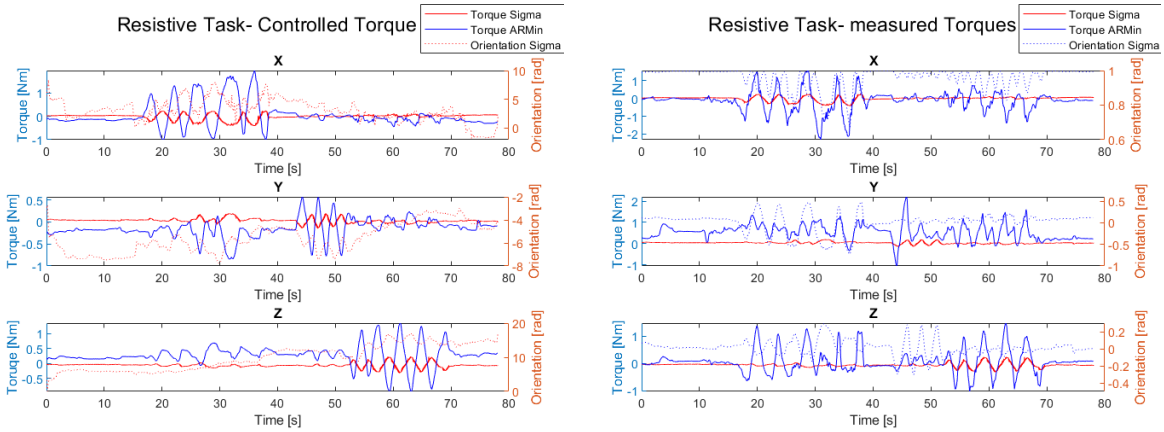

(a) Controlled

(b) Measured

Figure B.2: Torque Orientation plots, Resistive, Demonstrator: ARMin V

From figures B.1 and B.2 we can see the controlled en measured torques on the end-effectors for the resistive task. Noticeable is the order of magnitude, which is clearly lower for the measured torques in the ARMin V in the X and Z-direction. While in the Y-axis there is a bias visible of 0.5 Nm which can be attributed to compensating the weight of the arm. The best tracking when ARMin V is observing (fig B.1)appears to happen in the pronation-supination movement. When ARMin V is demonstrating we see that Sigma.7 only produces a Torque when the Torque in ARMin V is relatively high. However the magnitude of Torque for Sigma.7 is low, but a maximum of 0.4 Nm can be applied. Higher gains could thus be applied to the Sigma.7 side.

Sigma.7 has shown negligible low tracking errors, thus we will analyze the torque tracking error for the ARMin V as defined by B.1, where the $\tau_{measured}$ is obtained from the force-torque sensor on the end-effector of the ARMin V. From Figures B.3 and B.4 we see that tracking error improves when the ARMin V is demonstrating, but for both cases large torque tracking errors are present.

$$Error_{\tau} = \tau_{control} - \tau_{measured} \tag{B.1}$$

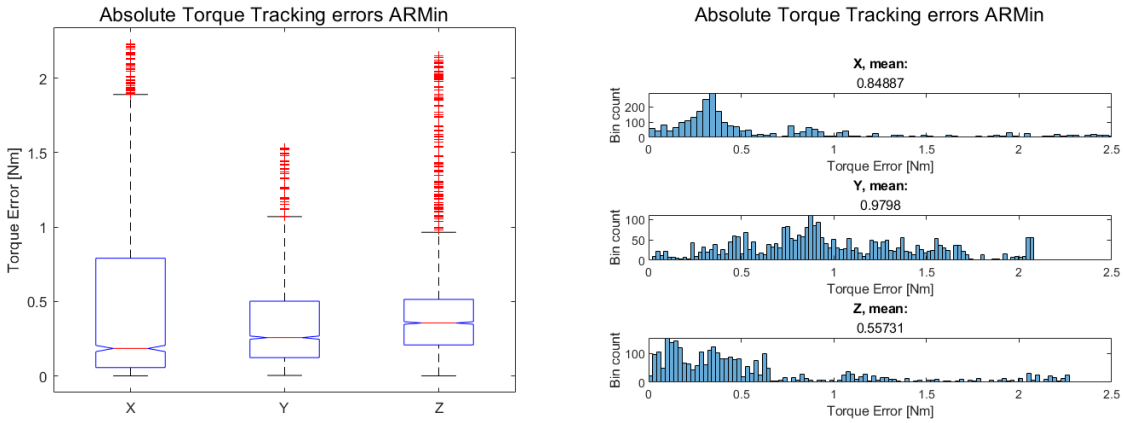

(a) Boxplot

(b) Histogram

Figure B.3: Absolute Torque tracking error, Resistive, Demonstrator: Sigma.7

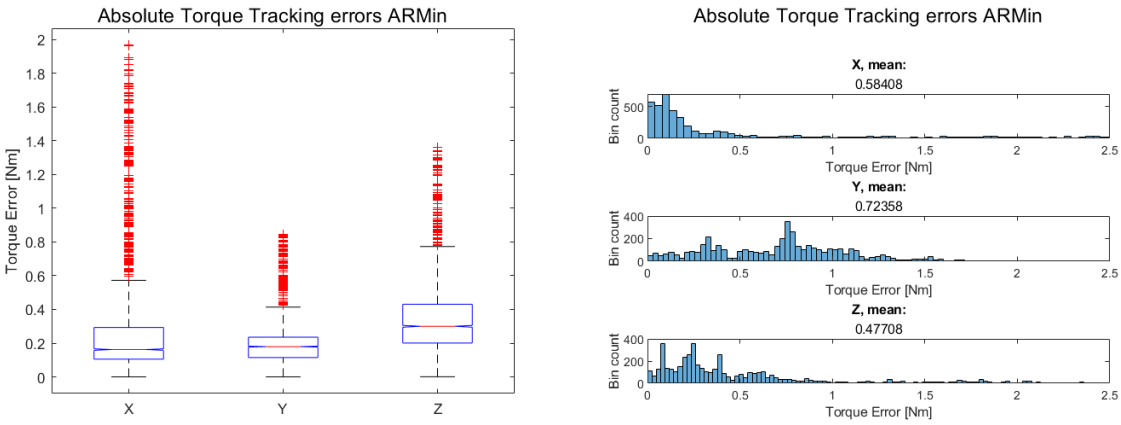

(a) Boxplot (b) Histogram

Figure B.4: Absolute Torque tracking error, Resistive, Demonstrator: ARMin V

B.2. Orientation plots, Compliant

When looking at Figures B.5 we can see that the Sigma.7 is able to track orientation of the ARMin V end-effector better then when the Sigma.7 is demonstrating. From Figure B.5b it can be seen that for the Z-axis the Sigma.7 is not able to track orientation to the full extent due to its workspace, which is not 360 degrees but [235, 140, 200] degrees “ForceControl.dvi - ForceControl.pdf”, n.d.

When looking at Figures B.5a and B.6a we can see that the ARMin V has trouble tracking the orientation, which could be explained by its kinematics. To orient the end-effector of the ARMin V multiple joints need to be moved to reach this orientation, while the orientation of the Sigma.7 end-effector is controlled in the end-effector itself. Thus the ARMin V is often delayed in its movement. Comparing the compliant passive task to the compliant active task we see that the ARMin V is able to track slightly better but is often fluctuating in orientation while the Sigma.7 remains constant. These results indicate that the torque translated from the ARMin V end-effector to the joint torques is not high enough for some joints such that the end-effector is able to track orientation correctly.

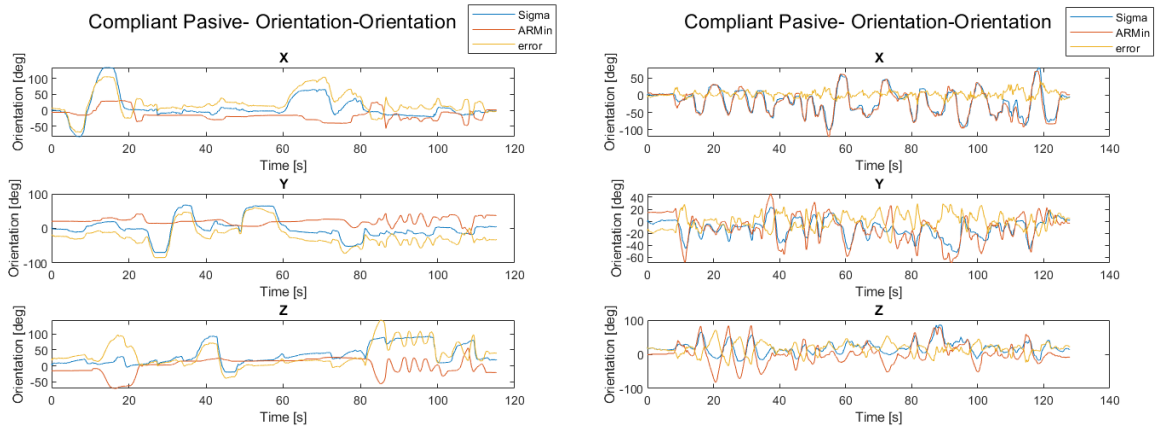

(a) Demonstrator: Sigma.7 (b) Demonstrator: ARMin V

Figure B.5: Orientation-Orientation plots, Compliant Passive

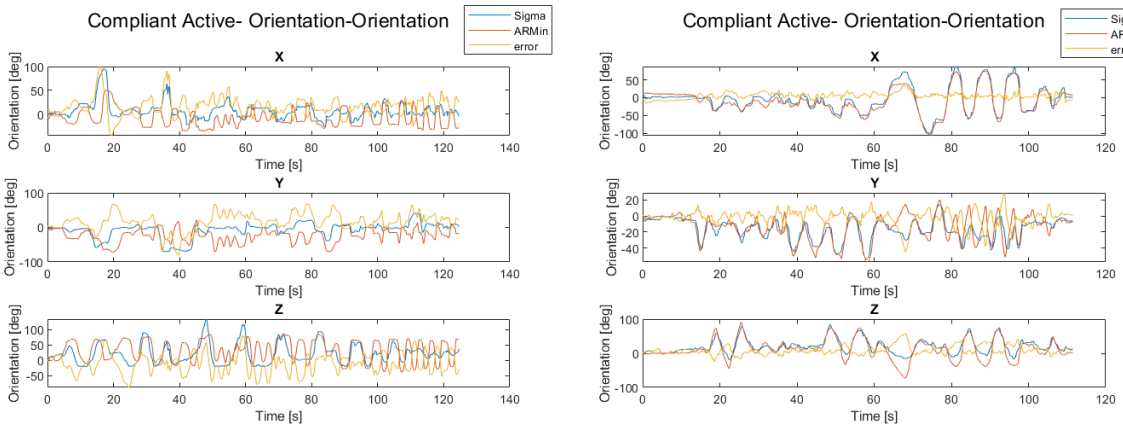

(a) Demonstrator: Sigma.7

(b) Demonstrator: ARMin V

Figure B.6: Orientation-Orientation plots, Compliant Active

B.3. Torque Plots, Compliant

From Figure B.6 we see that when ARMin V is observing the reaction in the X and Y directions is slow. This is also visible in Figure B.5 here however there is often no Torque reaction on the ARMin V when observing. However, when the ARMin V is demonstrating Sigma.7 produces only a small tracking error. Most noticeable from Figures B.7 and B.8 is the large difference in magnitude of torque. While Sigma.7 has a maximum torque of 0.4 Nm does not seem to reach these values. Secondly, a large difference between the recorded and measured torque for the ARMin V is visible. This is due to the joint kinematics of ARMin V and the force-torque sensor used for the measured force. Only the end-effector force-torque sensor was used for the measured torque, however, when controlled torque on the end-effector is translated to joint torques it also applies torque to joints that are not recorded by the end-effector force-torque sensor.

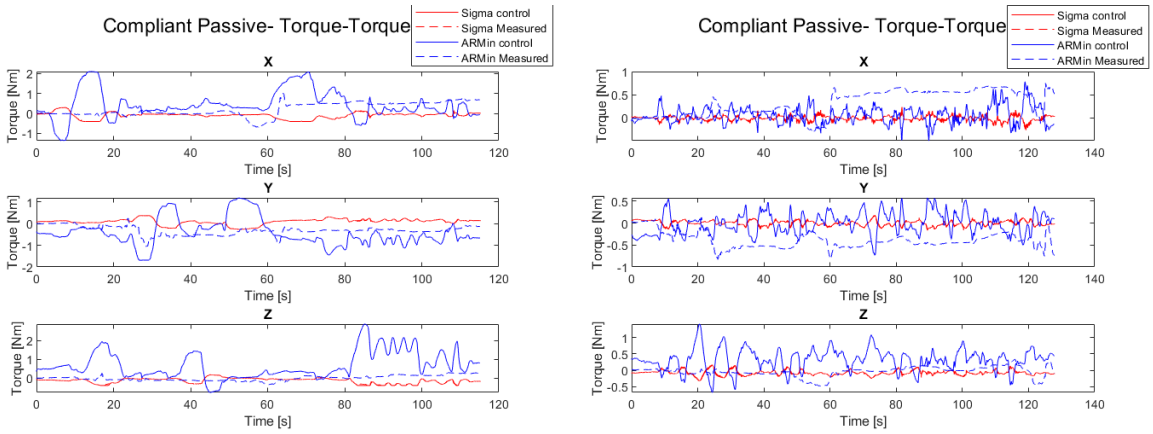

(a) Demonstrator: Sigma.7

(b) Demonstrator: ARMin V

Figure B.7: Torque-Torque plots, Compliant Passive

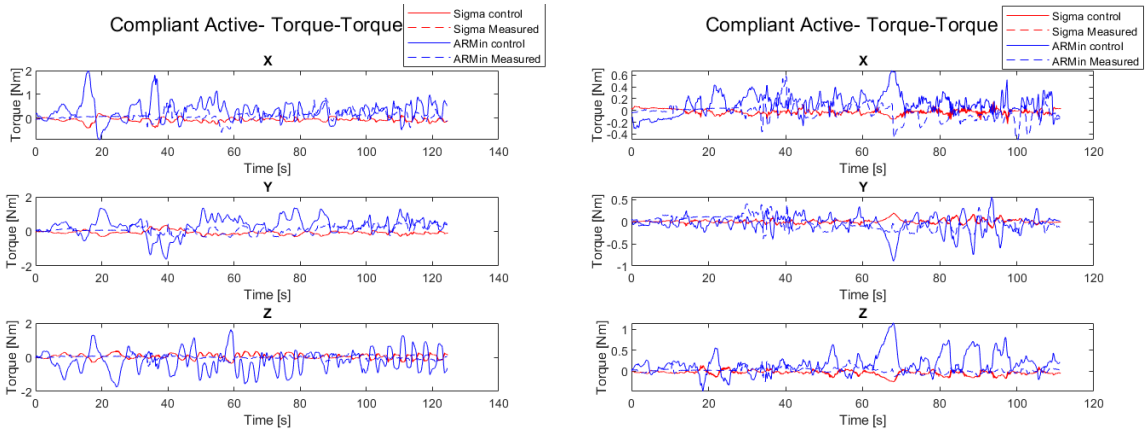

(a) Demonstrator: Sigma.7

(b) Demonstrator: ARMin V

Figure B.8: Torque-Torque plots, Compliant Active

B.4. Impedance, Compliant

To calculate the impedance ratio first the individual impedances for the ARMin V and Sigma.7 are calculated by $Z = \frac{\tau}{\omega}$. Impedance is a measure of how much the system resists motion when subjected to a harmonic force and is evaluated in the frequency domain. Lower impedance means that the system needs less force to move the system with the desired velocity. The individual impedances calculated are a combination of the robot (kinematics and local control), its operator, and teleoperation control. First angular velocity is calculated for both robots, then torque and angular velocity are transformed from the time domain to the frequency domain using the fast Fourier transform (FFT) function of Matlab R2020b. When calculating the impedance ratio first the frequency vectors for torque and angular velocity of the Sigma.7 are sampled down to match the ARMin V. From these sampled down vectors the impedance is calculated for the Sigma.7. The impedance ratio is calculated by Equation B.2. Due to velocity filtering for the Sigma.7 the impedance is only analyzed up to the cut-off frequency of the low-pass filter, which was 20 Hz for torque-orientation control (Section C.6).

$$Z_{ratio} = \frac{Z_{demonstrator}}{Z_{observer}} \tag{B.2}$$

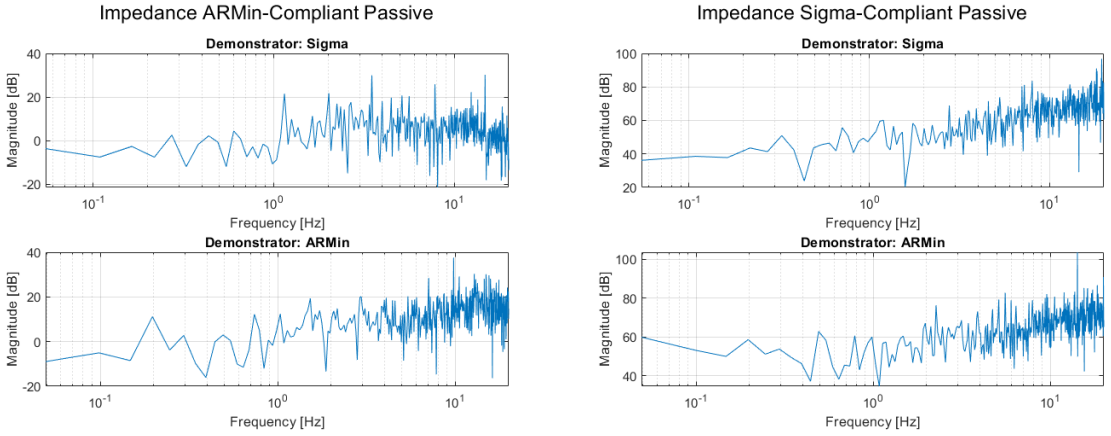

(a) Impedance ARMin V

(b) Impedance Sigma.7

Figure B.9: Impedance individual robots, Compliant Passive

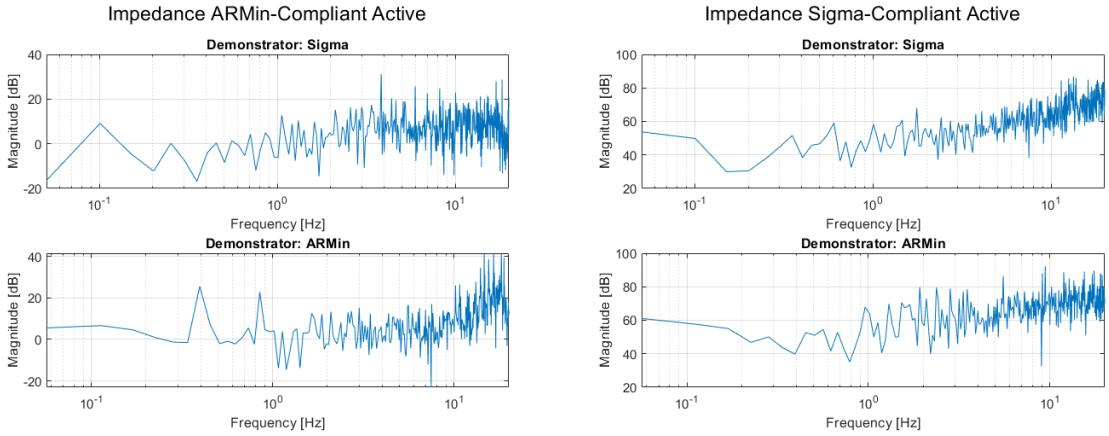

(a) Impedance ARMin V

(b) Impedance Sigma.7

Figure B.10: Impedance individual robots, Compliant Active

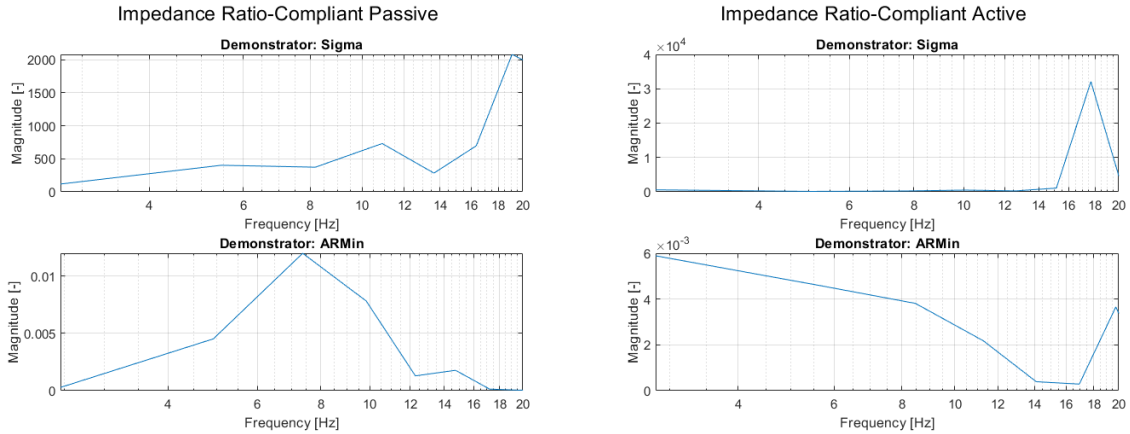

(a) Compliant Passive

(b) Compliant Active

Figure B.11: Impedance Ratio

B.5. Tracking Error

Orientation tracking error is defined by Equation B.3 (with Q=orientation in degrees). From Figures B.12-B.15 it can be seen that Sigma.7 is able to track ARMin V better than the ARMin V is able to track the Sigma.7. Which matches results found in both force-position control, and from the orientation-orientation plots.

$$Error_Q = Q_{demonstrator} - Q_{observer} \tag{B.3}$$

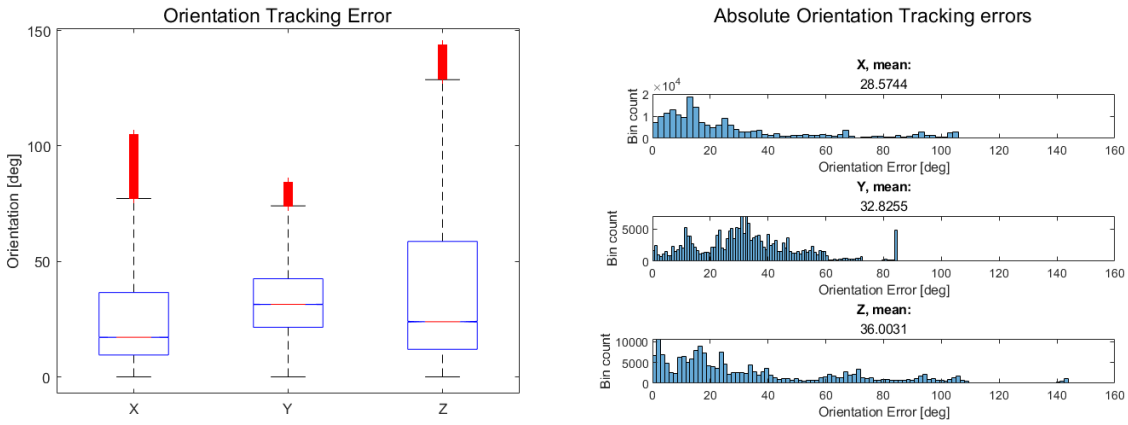

(a) Boxplot (b) Histogram

Figure B.12: Orientation tracking error, Compliant Passive, Demonstrator: Sigma.7

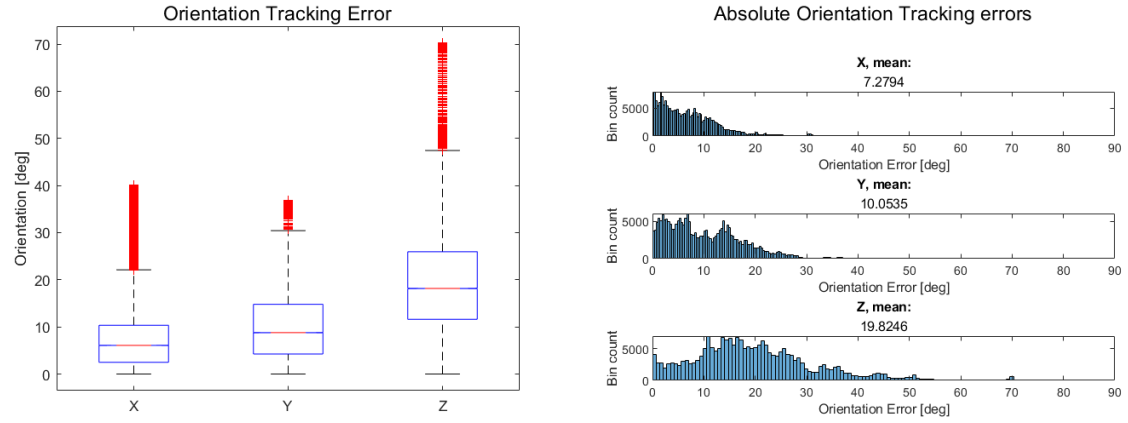

(a) Boxplot (b) Histogram

Figure B.13: Orientation tracking error, Compliant Passive, Demonstrator: ARMin V

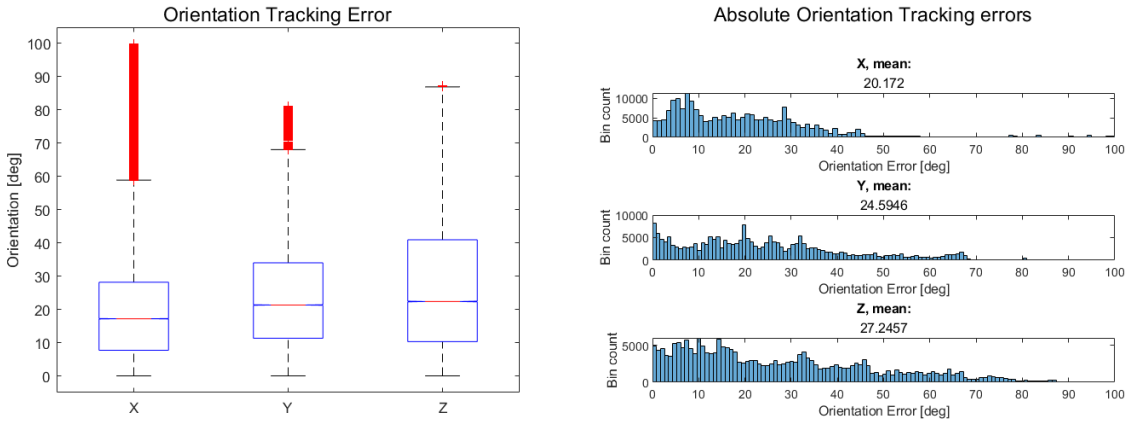

(a) Boxplot (b) Histogram

Figure B.14: Orientation tracking error, Compliant Active, Demonstrator: Sigma.7

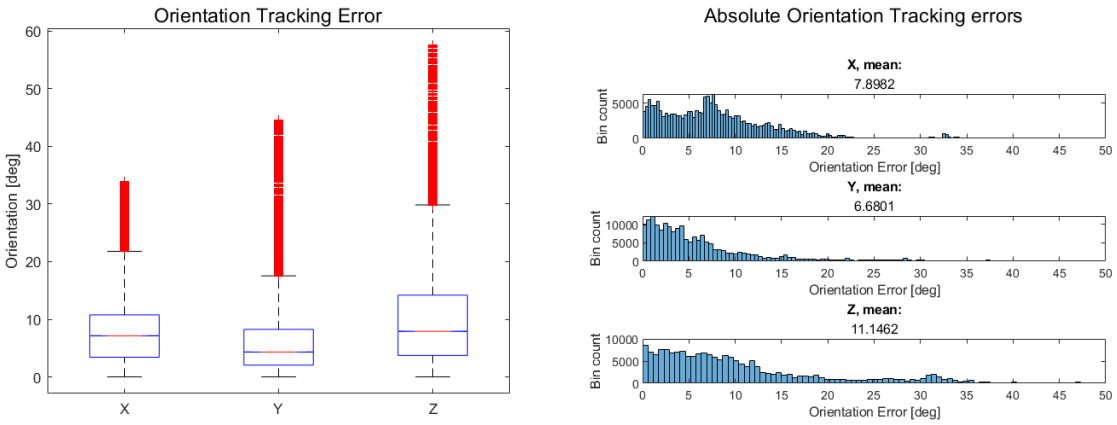

(a) Boxplot

(b) Histogram

Figure B.15: Orientation tracking error, Compliant Active, Demonstrator: ARMin V

B.6. Conclusion

From experiments, we could conclude that the orientation of the ARMin V is hard to control. Contrary to the Sigma.7 the ARMin V needs to move multiple joints to reach a certain orientation of the end-effector. Especially with high inertia to overcome in moving the shoulder joint which is especially visible when looking at the Z-axis. These results are in line with the results from force-position control, where movement caused by the shoulder joint (Y-axis for force-position control, Z-axis for torque-orientation control) is not tracking well. When comparing the tracking Figures B.12a and B.14a we see that the error is reduced for the active task. Especially errors around the Z-axis, which requires the shoulder joint, improved. This indicates that the torque provided by the demonstrator is interpretable for the observer. Which is in the same line as the results obtained from force-position control.

C

Other Results

C.1. Impedance, Force-Position control

Before calculating the impedance ratio we first calculated the individual impedances of both the ARMin V and Sigma.7. Due to filtering of the velocity of the Sigma.7, in which a cutoff frequency of 15 Hz was used, we only looked at a frequency domain between 0-15 Hz (Section C.6).

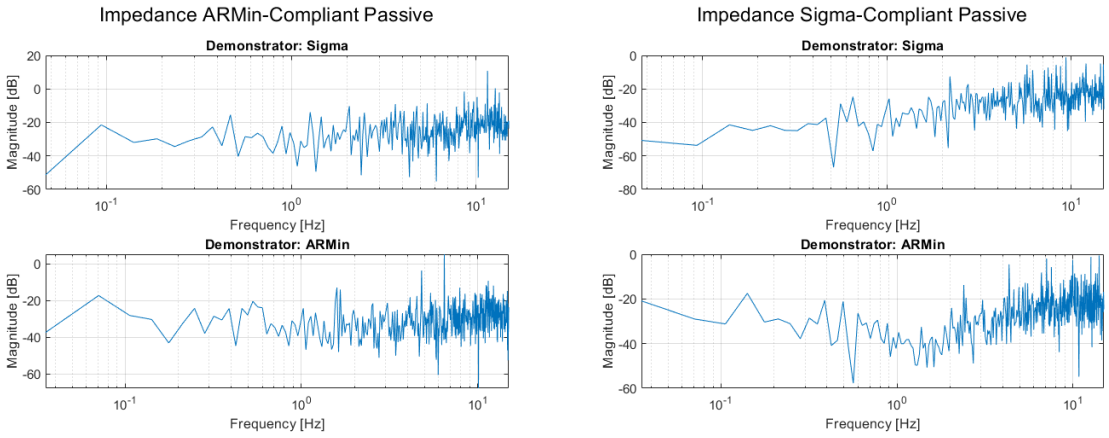

(a) Z_{ARMin} (b) Z_{Sigma}

Figure C.1: Impedances, Compliant Passive

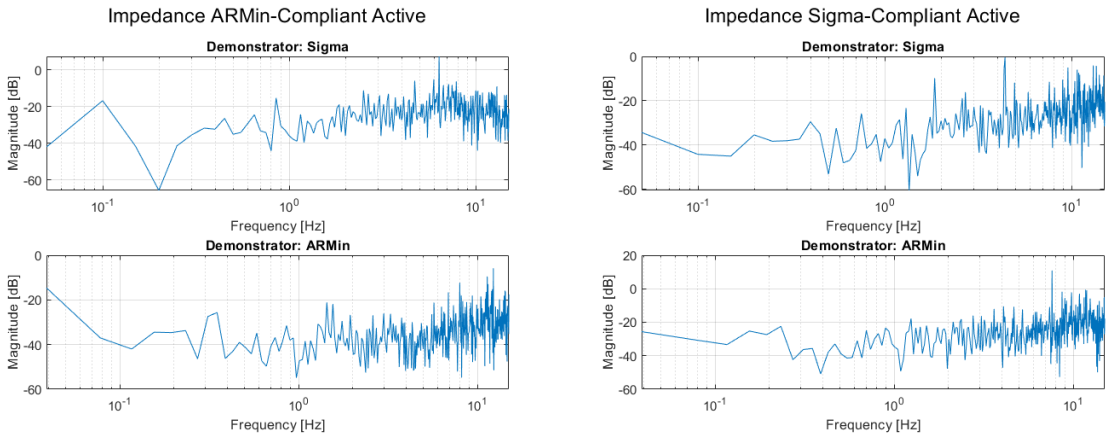

(a) Z_{ARMin} (b) Z_{Sigma}

Figure C.2: Impedances, Compliant Active

C.2. Position Tracking Errors

To evaluate how well the system performed based on low-level empirical evidence we evaluated the position tracking. The position tracking error is the difference in position between the ARMin V and Sigma.7. Where the Sigma.7 position is scaled (factor 10) to fit the same workspace and the origins of both devices overlap. As the boxplot did not provide clear insight into the amount of outliers present it was also chosen to use a histogram to see the distribution of the position tracking error.

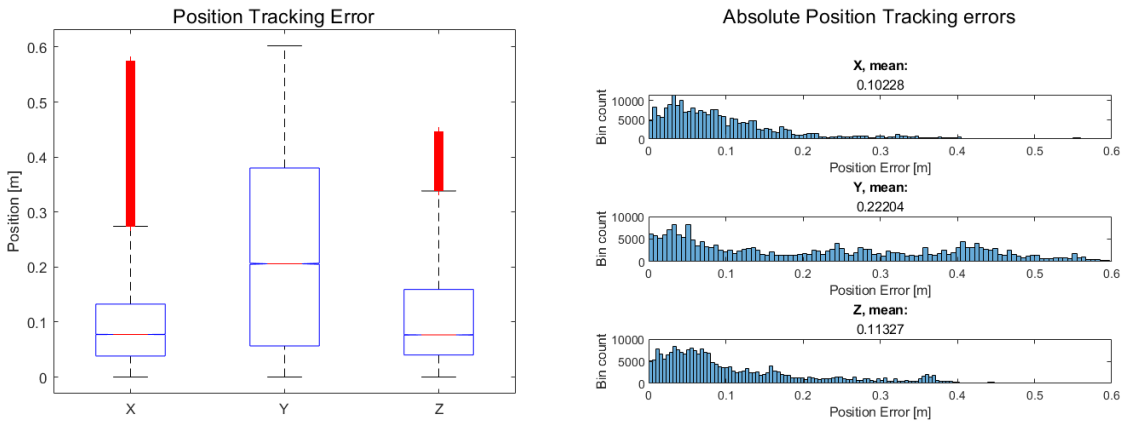

(a) Boxplot (b) Histogram

Figure C.3: Position Tracking errors, Compliant Passive, Demonstrator: Sigma.7

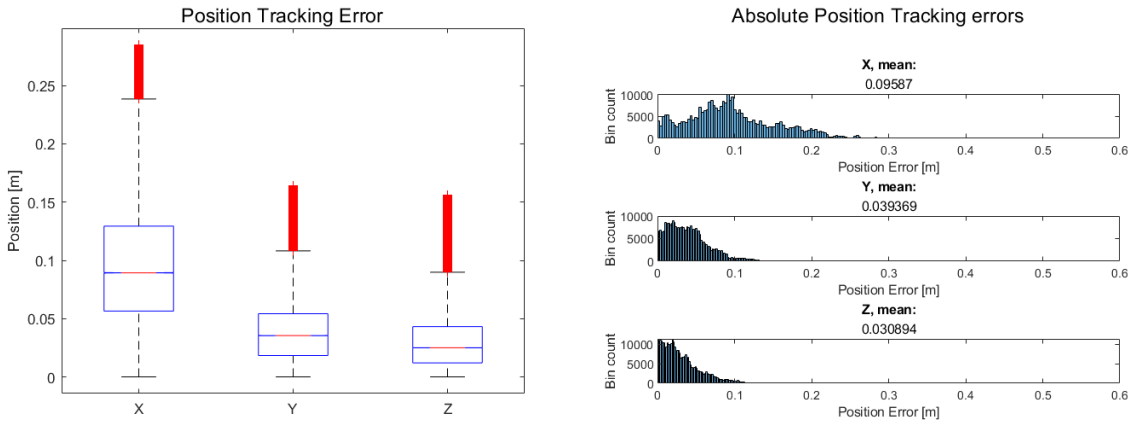

(a) Boxplot (b) Histogram

Figure C.4: Position Tracking errors, Compliant Passive, Demonstrator: ARMin V

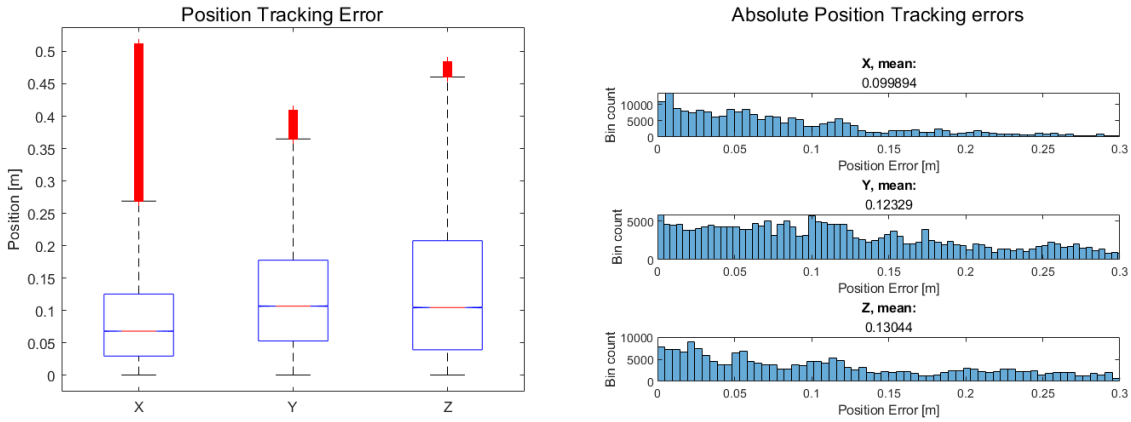

(a) Boxplot (b) Histogram

Figure C.5: Position Tracking errors, Compliant Active, Demonstrator: Sigma.7

C.3. Force-Force Plots

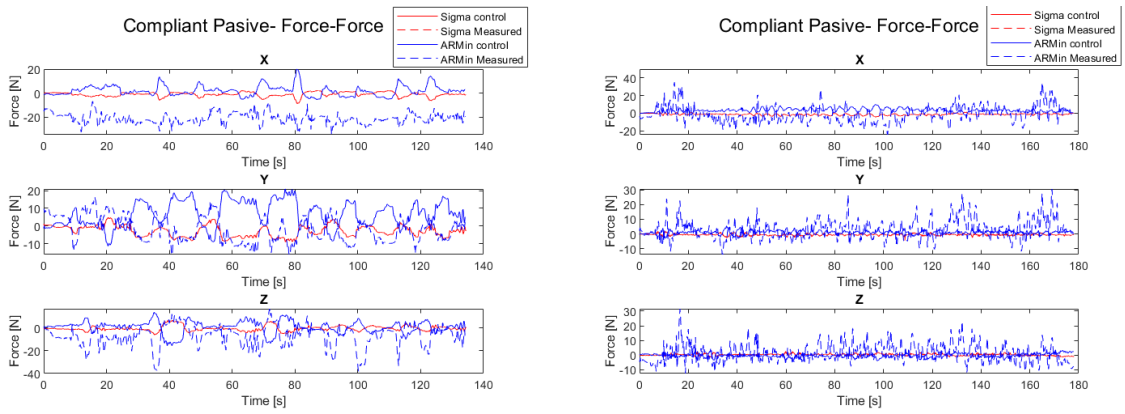

(a) Demonstrator Sigma.7 (b) Demonstrator ARMin V

Figure C.7: Force plots Compliant Passive

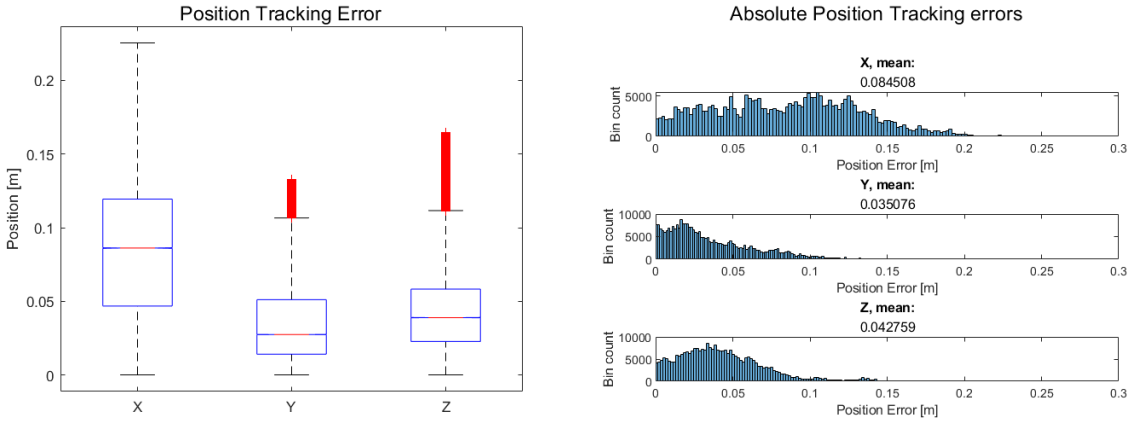

(a) Boxplot (b) Histogram

Figure C.6: Position Tracking errors, Compliant Active, Demonstrator: ARMin V

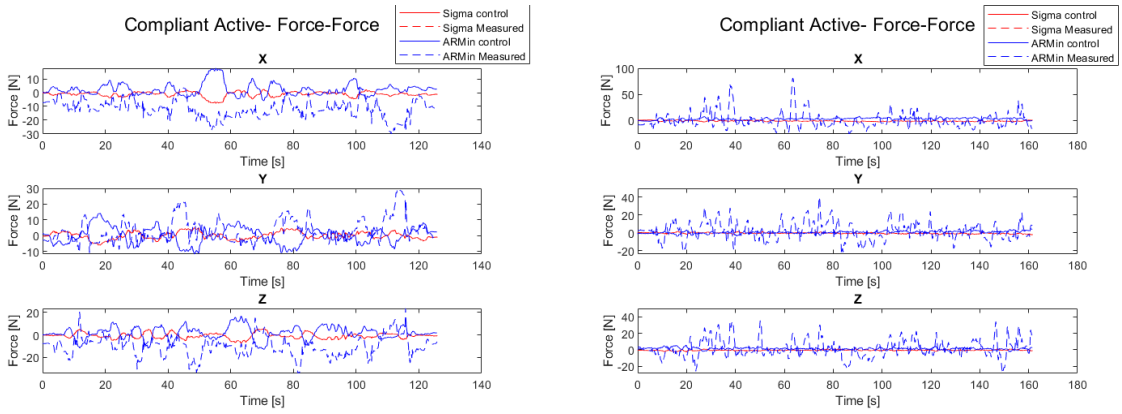

(a) Demonstrator Sigma.7 (b) Demonstrator ARMin V

Figure C.8: Force plots Compliant Active

C.4. Force Tracking Errors

In the resistive experiment, we evaluate the force tracking between the controlled and measured forces for both devices.

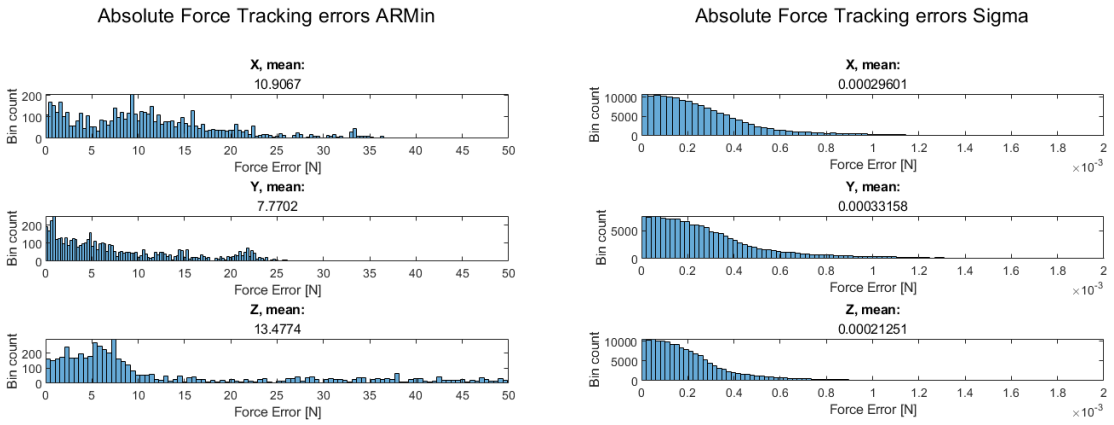

(a) ARMin V (b) Sigma.7

Figure C.9: Absolute Force Tracking errors-Demonstrator: Sigma.7

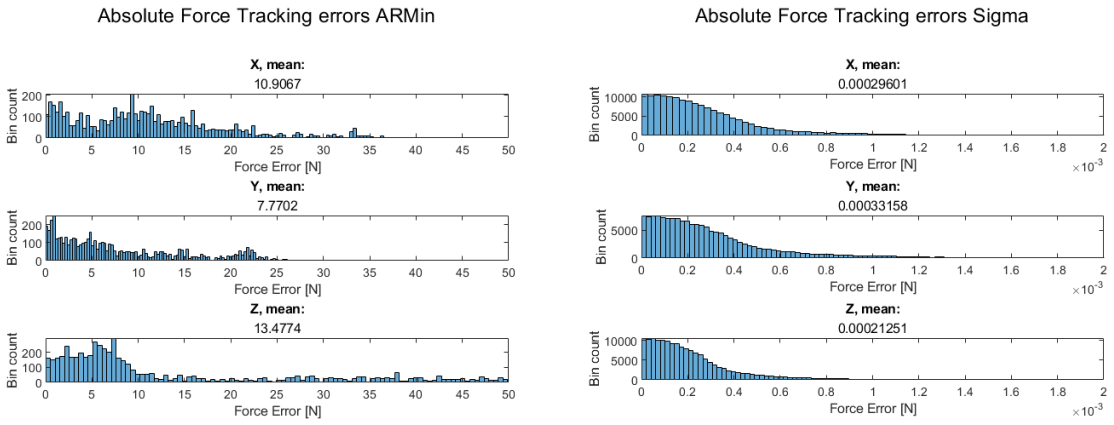

(a) ARMin V (b) Sigma.7

Figure C.10: Absolute Force Tracking errors-Demonstrator: ARMin V

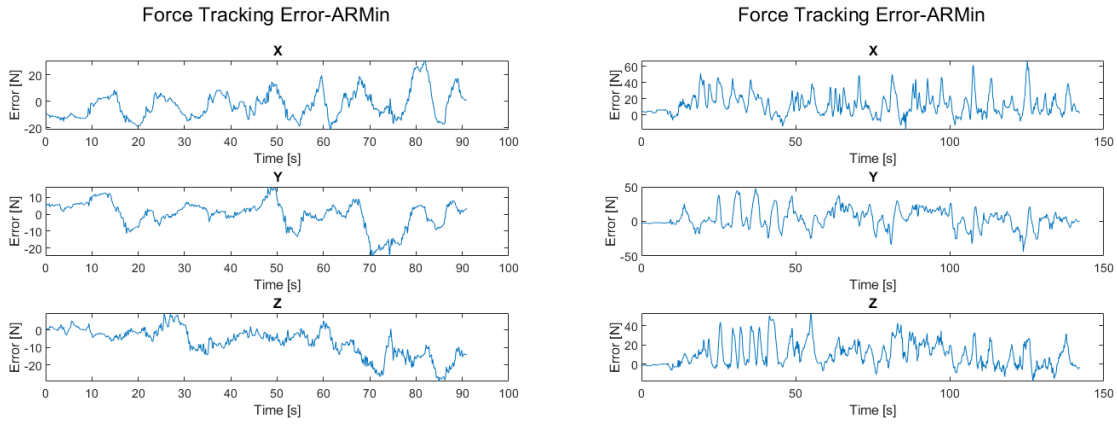

(a) Demonstrator: Sigma.7 (b) Demonstrator: ARMin V

Figure C.11: Force Tracking errors ARMin V

C.5. PD Values

As mentioned in the scientific paper the Proportional Derivative (PD) values were chosen empirically. However, some graphical analysis was performed when determining the PD values for the Sigma.7 side. This was done by connecting to the origin instead of the ARMin V and moving away from this point. Results were recorded and plotted to analyze oscillations. Not all force-position plots for all PD values are displayed here. Only the most interesting ones around the chosen PD values are displayed. The position displayed is the already scaled position for the Sigma.7.

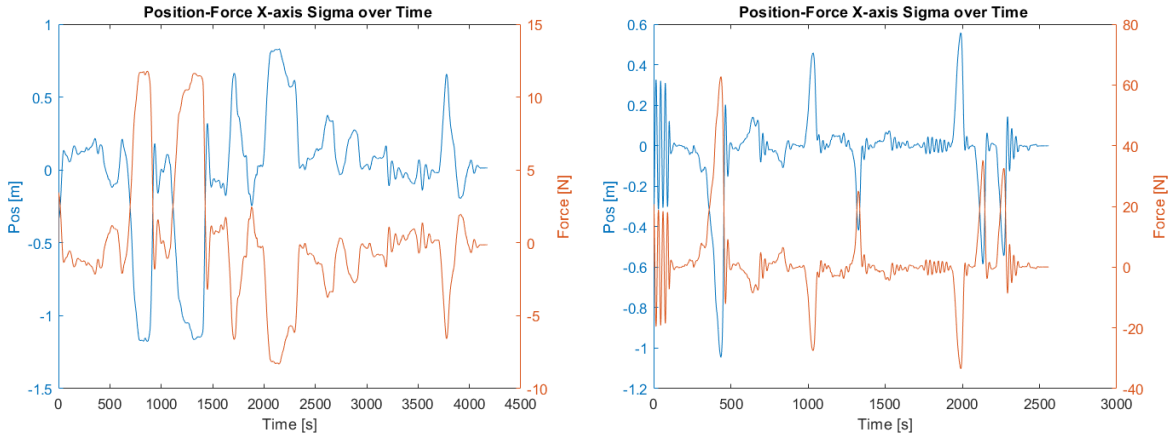

(a) P=10 N/m, B=0 Ns/m (b) P=10 N/m,B=5 Ns/m

Figure C.12: Position-Force plots Sigma.7

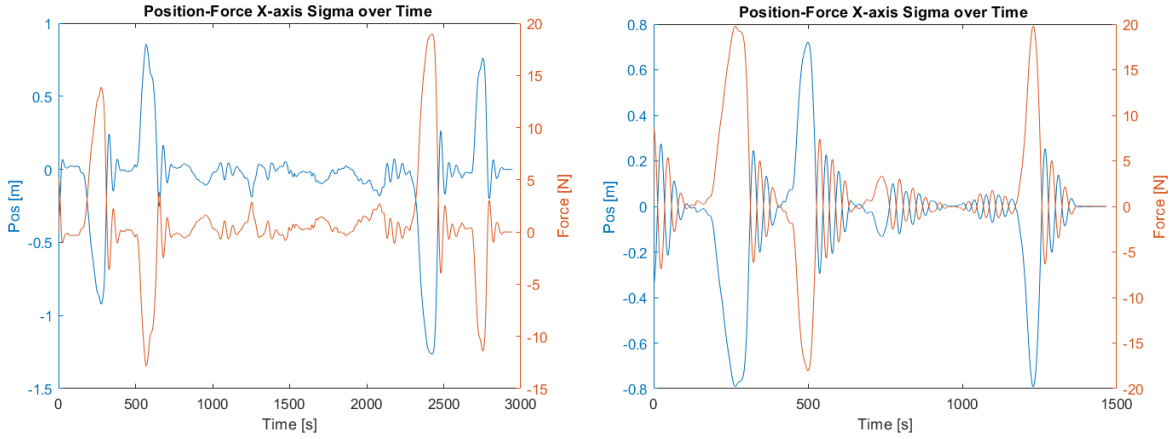

(a) P=15 N/m, B=0 Ns/m (b) P=25 N/m,B=0 Ns/m

Figure C.13: Position-Force plots Sigma.7

C.5.1. Discussion

The Sigma.7 has a maximum force of 20 N, which we are trying to reach when there is a maximum difference in position. From Figure C.12a we see that this value is not reached, however, with adding a Damping of 5 Ns/m (Figure C.12b), there is a peak in force present of 80 N. When we look at Figure C.13b we see that this 20 N is reached at its peaks. However, after every peak, oscillations are clearly visible, rendering the system very much unstable. Eventually, a proportional value of 15 N/m was chosen (Figure C.13a), and dampening was added according to Lee and Spong, 2006.

C.6. Velocity Filtering

When looking at the bode plots for ARMin V and Sigma.7 it was proposed to look into filtering the velocity of both robots. It was chosen to implement a first-order low-pass filter in Matlab R2020b. Therefore,

we first look into the frequency domain of the unfiltered velocities (Figure C.14) to investigate if any aliasing or noise is present. For the Sigma.7 we found a large magnitude at low frequency but aliasing occurs every 17 Hz. Thus a cut-off frequency of 15 Hz was chosen. For the ARMin V we also found a large magnitude at low frequency but aliasing occurred with decreasing magnitude around every 7.5 Hz, thus a cut-off frequency of 5 Hz was chosen. After filtering the velocities are analyzed again in the time domain (Figure C.15), comparing them to their unfiltered counterparts. It can be seen that the filtered velocity of the ARMin V falls exactly on top of the unfiltered velocity, showing no impact of filtering on the velocity. On the velocity of the Sigma.7, an effect can clearly be seen. From the zoomed-in x-axis, it can be seen that filtering has selected the correct envelope.

This analysis was repeated for torque-orientation control where absolute angular velocity was used instead of absolute velocity. It resulted in choosing a cut-off frequency of 20 Hz.

Due to the lack of effect of the velocity filtering for the ARMin V it was chosen to only filter the velocity of the Sigma.7. This filtered velocity is used to calculate the Impedance of Sigma.7 and the Impedance Ratio.

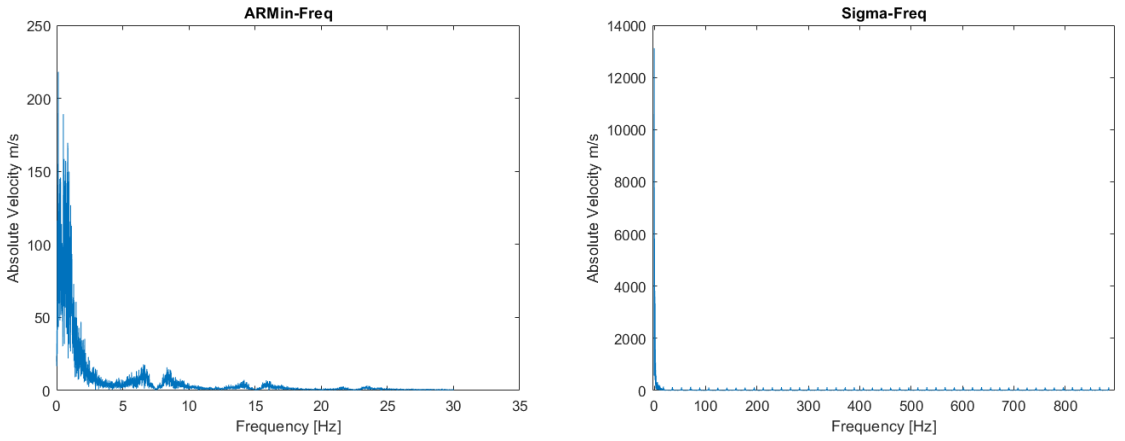

(a) Velocity ARMin V

(b) Velocity Sigma.7

Figure C.14: Unfiltered Velocities

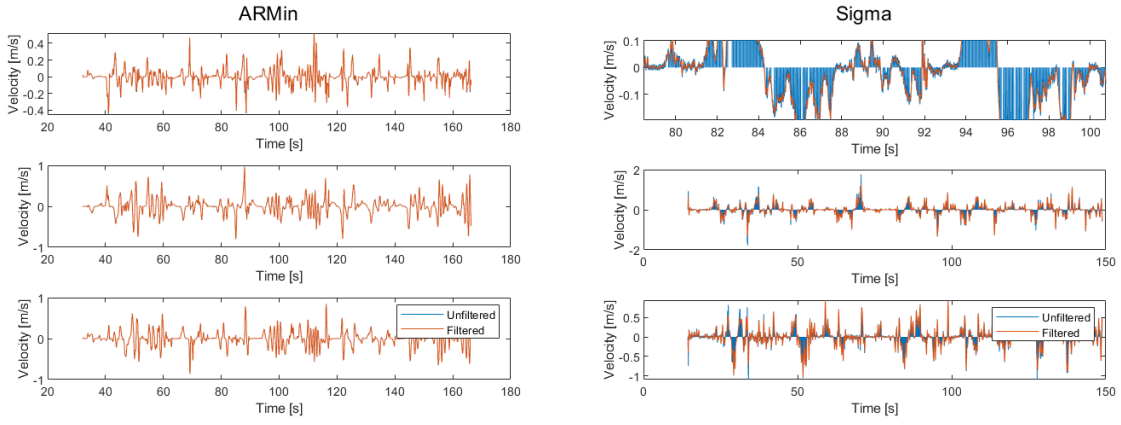

(a) Velocity ARMin V, cut-off=5 Hz

(b) Velocity Sigma.7, cut-off=15 Hz

Figure C.15: Filtered Velocities

C.7. Tracking Delay

To quantify how well the Sigma.7 and ARMin V are able to follow each other timing-wise it was decided to calculate the delay between the analyzed signals. This was done based on cross-correlation using Matlab R2020b C.16. Depending on the demonstrator and observer the observer and demonstrator

positions were assigned. The cross-correlation and matching delays (in the number of samples) were calculated per direction (X,Y,Z), and the index for the maximum cross-correlation was identified. Delay at maximum cross-correlation was calculated by using the lag at this maximum and multiplying it by the average time difference between samples. This method has however no guarantee of finding accurate delays, as force and position signals of the Sigma.7 and ARMin V are often less similar than desired, especially when the ARMin V is observing. This could lead to finding maximum cross-correlation on unrelated points in time, leading to a large or negative delay.

```
%StA:
obs_pos = eePosA_N;
dem_pos = eePosS;
% AtS:
%obs_pos=eePosS;
%dem_pos= eePosA_N;

[xc,lags_x]=xcorr(obs_pos(:,1),dem_pos(:,1));
[~,index_x]=max(xc);

dt=diff(time_S);
avg_dt=mean(dt);

dt_at_max_xc= lags_x(index_x)*avg_dt;
```

Figure C.16: Delay calculation, Matlab code

D

UDP Communication

To evaluate the UDP communication on its quality Wireshark is used to record the moments of communication. This data was used to calculate the minimum, maximum, and average dt values (between packages sent) per connection. From the average dt value, a frequency was calculated per experiment. Then this data was averaged over the 6 datasets resulting in Table D.1.

	Max (dt)	**Min (dt)**	**avg (dt)**	**avg (freq)**
LtH_H	0.02542	0	0.00031397	3210.6445
LtH_L	4.32249	1.28E-05	0.00039686	2949.5607
TtH	0.06221	1.33E-06	0.00022204	4802.6439
HtT	0.02183	3.33E-07	0.00029769	3372.2207
HtL_H	1.68406	0.009045	0.011268	88.750483
HtL_L	3.45226	0.008993	0.01143133	87.560867

Table D.1: UDP Updaterates (dt [s])

From the UDP update rates, the most noticeable are the Linux to Host connection (with a minimum dt of 0 s and a maximum dt of 4.3 s) and the low average frequency of the Host to Linux connection. Thus a deeper look into the distribution of dt values was needed.

D.1. evaluation Update rate

Due to the low UDP update rate from Host to Linux, we evaluated the dt, by taking the time difference between 2 send packages. This was done to check if the problem was constant or if outliers often influenced frequency. The experiment dataset compliant active for force-position control was used as this displayed the most problems. But as can be seen in Figure D.1 it is a very constant problem. But even though Linux to Host connection showed a high max dt we can see a more constant low magnitude for dt. When analyzing the update rates for all connections one figure stood out, Linux to Host connection as recorded on Linux (Fig. D.3). In this figure, we clearly see three parts where the value for dt is higher. These parts coincide with the moments when there is no connection (no grasping) between the two devices, and thus the inner loop is not running. And as the secondary loop has two moments of updating the UDP Packages there are two ranges of magnitude for dt, the time from the beginning to the end of the secondary loop, and the time from the end of the loop until the loop starts again.

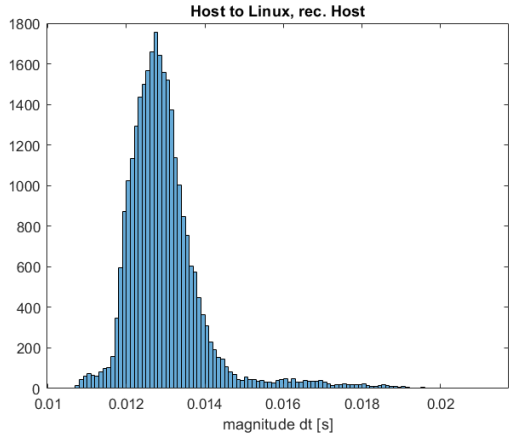

(a) As recorded on Host

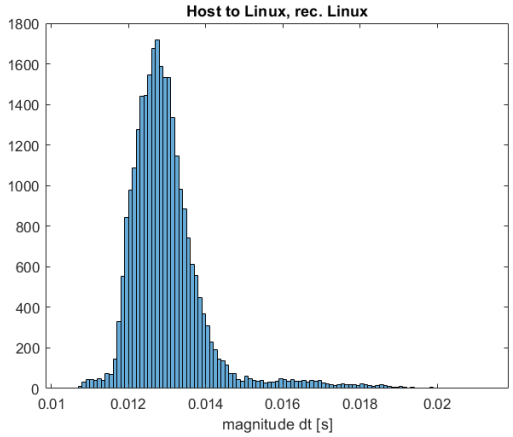

(b) As recorded on Linux

Figure D.1: dt Host to Linux, experiment Compliant Active-force controlled

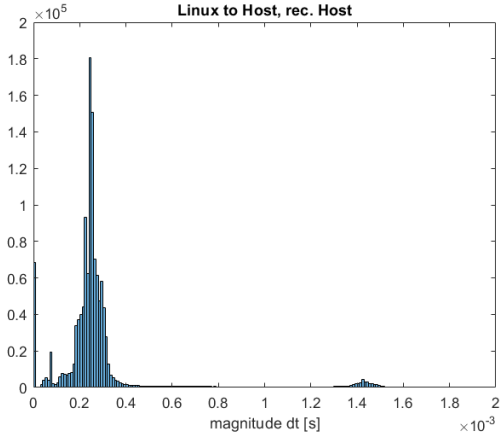

(a) As recorded on Host

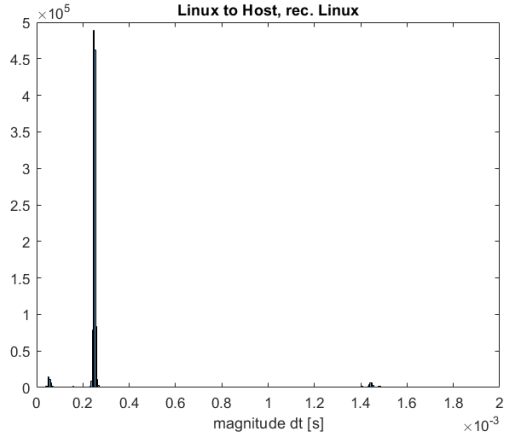

(b) As recorded on Linux

Figure D.2: dt Linux to Host, experiment Compliant Active-force controlled

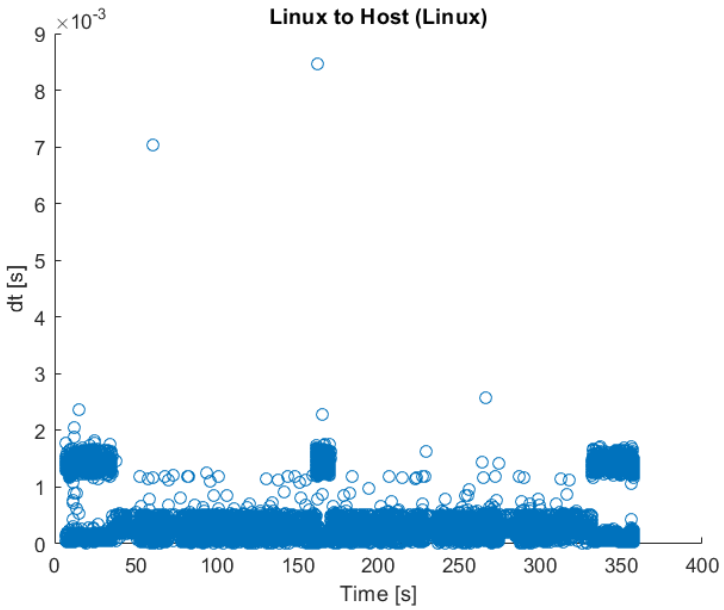

Figure D.3: dt over Time for Linux to Host, rec. Linux

E

Informed Consent Form

Delft University of Technology

HUMAN RESEARCH ETHICS
INFORMED CONSENT

Version 23/5/2023

Proof of concept study for a Tele-Rehabilitation system for Upper-Limb rehabilitation Exoskeleton.

Participant Information

You are being invited to participate in a research study titled "Proof of concept study for a Tele-Rehabilitation system for Upper-Limb Rehabilitation Exoskeleton". This study is being performed at the Motor Learning and Neurorehabilitation (MLN) Laboratory at the TU Delft, Cognitive Robotics Department.

The purpose of this study is to evaluate the telerehabilitation system on stability and transparency. The study will take approximately 120 minutes.

In this experiment, you will use either the ARMin exoskeleton, a prototype of an upper-limb robotic device for neurorehabilitation, or the Sigma.7, an end-effector haptic device. The robots will be operated in connected mode with each other. You will be asked to perform a dynamic task and a motion-resisting task. You will receive visual feedback displayed on a monitor or through the use of head-mounted displays. An experimenter will always be present and you will receive specific instructions before the experiment.

During the experiment, we will record a signal from the robot's kinematic and force/torque interaction sensors. The data will be used for further development of the system, reports, publications, presentations, and teaching. This data will be stored anonymously, and can be asked to be destroyed until publishing.

Because the device that you will test is a prototype, it cannot be excluded that a failure or malfunction occurs, which could potentially result in discomfort. Otherwise, no physical, emotional, or reputational risks are expected. Although the haptic forces that you will experience during the experiment are low, risks of minor injury during the interaction with the robot have been mitigated by following safety procedures in accordance with the TU Delft safety protocol.

During the experiment, you may experience minor muscular fatigue or discomfort in your arm, mitigated by several pauses between trials. There is a risk of Covid-19 transmission through equipment surfaces or face-to-face encounters, mitigated by disinfection of the robot. Additionally, your personal data and your answers will remain confidential and we will pseudo-anonymize your collected data prior to the publication of the study.

Your participation in this study is entirely voluntary and you can withdraw at any time during the experiment. You are free to omit any questions. You have the right to request access to and/or deletion of your collected data until one month after your participation, before the publication of the study. In case of any questions or requests, contact:

Nikki Korzilius – Msc Student

Alex van den Berg – Daily Supervisor

Dr. Laura Marchal-Crespo – Supervisor

Participant Information:

Name: _____

Date of Birth: _____

Gender: _____

E-mail Address: _____

Explicit Consent Points

PLEASE TICK THE APPROPRIATE BOXES	Yes	No
A: GENERAL AGREEMENT – RESEARCH GOALS, PARTICPANT TASKS AND VOLUNTARY PARTICIPATION		
1. I have read and understood the study information dated [*20/06/2023*], or it has been read to me. I have been able to ask questions about the study and my questions have been answered to my satisfaction.	☐	☐
2. I consent voluntarily to be a participant in this study and understand that I can refuse to answer questions and I can withdraw from the study at any time, without having to give a reason.	☐	☐
3. I understand that taking part in the study involves: • I will receive instructions about the tasks and the systems that I will test • I will perform tasks with the Exoskeleton or Haptic device in an unsupervised scenario. The experimenter will always be present and I will receive specific instructions prior to the experiment but will be asked to perform the tasks by myself. • A computer monitor or (optional) head-mounted display will be used to display a task that has to be performed with the device. • The device is capable of generating haptic forces at the interaction point with the arm. While performing the tasks, I will feel the interaction forces through the device.	☐	☐
4. I understand that there will be no compensation for my participation	☐	☐
5. I understand that the study will take approximately 60 minutes	☐	☐
B: POTENTIAL RISKS OF PARTICIPATING (INCLUDING DATA PROTECTION)		
6. I understand that taking part in the study involves the following risks: • The Exoskeleton that is part of the system is a research prototype and not a CE-certified device. It can therefore not be excluded that a mechanical or electrical	☐	☐

PLEASE TICK THE APPROPRIATE BOXES	Yes	No
failure or a software malfunction occurs and I may experience a minor injury due to collision with the robot. • I may experience minor fatigue or discomfort in the arm during the tasks • I may experience exposure to COVID-19 I understand that these will be mitigated by: • An in-depth risk assessment was performed by the developers and the risks of injury were mitigated in accordance with the TU Delft protocol. For instance, the device is equipped with two emergency stop buttons. One is operated by me and the other one is operated by the experimenter. Pushing one of the emergency stop buttons will immediately power off the device. • Appropriate resting time is assigned between trials and I am always allowed to press the emergency stop button at any time without justification. • All equipment will be disinfected before and after use. All relevant Covid-19 regulations and recommendations of the Dutch government during the time of the experiment will be complied with.		
7. I understand that taking part in the study also involves collecting specific personally identifiable information (PII) such as name, age, and contact details and associated personally identifiable research data (PIRD) with the potential risk of my identity being revealed to all researchers involved in this study. No PII or PIRD will be made publicly available.	☐	☐
8. I understand that some of this PIRD are considered sensitive data within GDPR legislation, specifically • All data will be stored according to a data management plan that was developed and approved by an expert at TU Delft. • The collected data will be stored on a server located at the TU Delft. • The collected data will be pseudonymized. • The informed consent sheet will be stored on a server located at the TU Delft.	☐	☐
9. I understand that the following steps will be taken to minimize the threat of a data breach and protect my identity in the event of such a breach. - Data will be (pseudo-) anonymized. - Data will be stored on a server at the TU Delft - Videos and photos will only be used after consent.	☐	☐
Provide brief summaries of the mitigating measures to be taken (eg: anonymous data collection, (pseudo-) anonymisation or aggregation, secure data storage/limited access, transcription, blurring, voice modification etc)		

PLEASE TICK THE APPROPRIATE BOXES	Yes	No
10. I understand that personal information collected about me that can identify me, such as my name, my age, will not be shared beyond the study team.	☐	☐
11. I understand that the (identifiable) personal data I provide will be destroyed after publication of the study results.	☐	☐
C: RESEARCH PUBLICATION, DISSEMINATION AND APPLICATION		
12. I understand that after the research study the de-identified information I provide will be used for further development of the device, report(s), publication(s), presentation(s), and teaching	☐	☐
D: (LONGTERM) DATA STORAGE, ACCESS AND REUSE		
13. I give permission for the de-identified research data (e.g. task metrics, age) that I provide to be archived in 4TU Data Center repository so it can be used for future research and learning.	☐	☐
14. I understand that access to this repository is open	☐	☐

Signatures

_____	_____	_____
Name of participant [printed]	Signature	Date

I, as researcher, have accurately read out the information sheet to the potential participant and, to the best of my ability, ensured that the participant understands to what they are freely consenting.

_____	_____	_____
Researcher name [printed]	Signature	Date

Study contact details for further information: [*Name, phone number, email address*]

Nikki Korzilius

Bibliography

ForceControl.dvi - ForceControl.pdf. (n.d.).

Lee, D., & Spong, M. W. (2006). Passive bilateral teleoperation with constant time delays. *Proceedings - IEEE International Conference on Robotics and Automation*, *2006*(2), 2902–2907. https://doi.org/10.1109/ROBOT.2006.1642142

Lomba, T., & Marchal-Crespo, L. (2023). *Development of an upper limb exoskeleton digital twin in immersive virtual reality* (tech. rep.). Universidade de Lisboa.

Morris, D., Hong, T., Barbagli, F., Chang, T., & Salisbury, K. (2007). Haptic feedback enhances force skill learning. *Proceedings - Second Joint EuroHaptics Conference and Symposium on Haptic Interfaces for Virtual Environment and Teleoperator Systems, World Haptics 2007*, 21–26. https://doi.org/10.1109/WHC.2007.65